Journal of Genetics and Genomics xxx (xxxx) xxx

Contents lists available at ScienceDirect

Journal of Genetics and Genomics

Journal homepage: www.journals.elsevier.com/journal-of-genetics-and-genomics/

Method

Unveiling cell-type-specific mode of evolution in comparative single-cell expression data

Tian Qin [a, b], Hongjiu Zhang [c], Zhengting Zou [a, b, *]

[a] State Key Laboratory of Animal Biodiversity Conservation and Integrated Pest Management, Institute of Zoology, Chinese Academy of Sciences, Beijing 100101, China
[b] University of Chinese Academy of Sciences, Beijing 101408, China
[c] Microsoft Canada Development Centre, Vancouver, British Columbia, V5C 1G1, Canada

ARTICLE INFO

Article history:
Received 20 April 2025
Received in revised form
30 April 2025
Accepted 30 April 2025
Available online xxx

Keywords:
Singe-cell transcriptomics
Gene expression
Adaptive evolution
Cell type
Phenotypic evolution
Prefrontal cortex
Naked mole-rat

ABSTRACT

While methodology for determining the mode of evolution in coding sequences has been well established, evaluation of adaptation events in emerging types of phenotype data needs further development. Here, we propose an analysis framework (*e*xpression *va*riance *de*composition, EVaDe) for comparative single-cell expression data based on phenotypic evolution theory. After decomposing the gene expression variance into separate components, we use two strategies to identify genes exhibiting large between-taxon expression divergence and small within-cell-type expression noise in certain cell types, attributing this pattern to putative adaptive evolution. In a dataset of primate prefrontal cortex, we find that such human-specific key genes enrich with neurodevelopment-related functions, while most other genes exhibit neutral evolution patterns. Specific neuron types are found to harbor more of these key genes than other cell types, thus likely to have experienced more extensive adaptation. Reassuringly, at the molecular sequence level, the key genes are significantly associated with the rapidly evolving conserved non-coding elements. An additional case analysis comparing the naked mole-rat (NMR) with the mouse suggests that innate-immunity-related genes and cell types have undergone putative expression adaptation in NMR. Overall, the EVaDe framework may effectively probe adaptive evolution mode in single-cell expression data.

Introduction

Adaptation of living organisms to their environment is realized by evolutionary changes of phenotypes. Since the seminal finding of high protein sequence similarity between species by King and Wilson (1975), the regulation of gene expression has been considered as a major molecular basis underlying adaptive phenotypic divergence, with extensive evidence reported (Gilad et al., 2006a; Carroll, 2008; Necsulea and Kaessmann, 2014). For example, the skin-specific up-regulation of *Agouti* gene expression causes a larger ventrum area with lighter coloration in beach-dwelling deer mice, thus being advantageous and adaptive in the light-colored sand dune environment (Manceau et al., 2011). Hence, although it remains unclear whether gene expression evolution is dominated by neutral or adaptive factors, as a type of molecular phenotype, it is known that transcriptomic data contain information on organismal adaptation (Whitehead and Crawford, 2006; Fay and Wittkopp, 2008; Fraser, 2011; Hodgins-Davis et al., 2015; Signor and Nuzhdin, 2018).

Given this significant relevance and the rapidly accumulating comparative transcriptomic data in recent years, various analysis strategies for detecting adaptive gene expression patterns have been developed. Apart from approaches that require genetic manipulations such as eQTL-mapping (Fraser, 2011), some studies compared between-species divergence and within-species variation of gene expression to evaluate adaptation (Rifkin et al., 2003; Khaitovich et al., 2005; Gilad et al., 2006b; Whitehead and Crawford, 2006), analogous to the Hudson-Kreitman-Aguadé (HKA) test in sequence evolution (Hudson et al., 1987). For example, Rifkin et al. (2003) designed consecutive tests to categorize expression patterns into different evolutionary modes for 6742 *Drosophila* genes, among which 1729 varied little within species but more between species and were considered as being under species-specific

* Corresponding author.
E-mail address: zouzhengting@ioz.ac.cn (Z. Zou).

https://doi.org/10.1016/j.jgg.2025.04.022

selection. In another study by Gilad et al. (2006b), a linear mixture model was used to discriminate between-species divergence of primate gene expression and the random effect of within-species variation. Nineteen out of 110 genes were found to show high between-species variance relative to within-species variance, and were considered as having experienced directional selection during human evolution. Meanwhile, traditional evolution models of continuous traits have also been widely adopted in detecting evolution modes of gene expression, such as Brownian motion, Ornstein–Uhlenbeck and their variants (Rohlfs et al., 2014; Rohlfs and Nielsen, 2015; Yang et al., 2019; Bertram et al., 2023). Some of these models also explicitly parameterize the between- versus within-species variance ratio to reflect distinct evolution modes such as adaptation (Rohlfs and Nielsen, 2015). However, comparative approaches relying on expression data from bulk assays may share some common challenges. For example, different tissue allometries in two species may appear to be differential expression, and the same is true for different cell type compositions in the same tissue of two species (Price et al., 2022).

Single-cell expression data provide a further layer of cell type information, and thus could potentially avoid such biases. In the last decade, expression data from single-cell RNA sequencing assays have been fast accumulating, from comprehensive cell type atlases (Regev et al., 2017; Consortium, 2018; Plass et al., 2018) to investigations of cell types in specific tissues, diseases, or development stages (Ximerakis et al., 2019; Elmentaite et al., 2022). Specifically, there have been comparative studies analyzing single-cell expression data across different species (La Manno et al., 2016; Tosches et al., 2018; Geirsdottir et al., 2019; Hodge et al., 2019; Wang et al., 2021; Ma et al., 2022; Shafer et al., 2022; Jorstad et al., 2023; Murat et al., 2023; Suresh et al., 2023). With cell type inference for each single cell, the difference in cell type compositions is less confounding, as the inferred cell population of a specific type can be directly compared between species. However, it remains unclear how to identify the mode of evolution (neutral or adaptive) using comparative single-cell expression data. In order to demonstrate potentially adaptive cellular level changes across species or lineages, most comparative studies focus on species- or lineage-specific cell types (Wang et al., 2021; Ma et al., 2022; Shafer et al., 2022; Niepoth et al., 2024) or differential expression of gene sets (Bakken et al., 2021; Ma et al., 2022; Shafer et al., 2022; Jorstad et al., 2023; Suresh et al., 2023). Additionally, some studies associate differentially expressed genes (DEGs) with genome regions of high divergence levels (Gao et al., 2022; Jorstad et al., 2023; Murat et al., 2023). While testing for DEGs is a conventional approach to identify sample-specific gene expression, the commonly used pseudo-bulk or meta-cell grouping diminishes the between-cell heterogeneity information. Moreover, both neutral and adaptive evolution processes may drive divergence of expression for an individual gene within a specific cell type, resulting in the pattern of differential expression (Bakken et al., 2021; Callaway et al., 2021; Lee et al., 2025). Overall, there are few statistical frameworks for explicitly investigating the mode of evolution reflected by comparative single-cell expression data.

Given the aforementioned challenges in detecting adaptive expression evolution, we explore another existing approach (Ho et al., 2017). This approach states that important traits should evolve slower under neutral evolution. Hence, if the between-species divergence of a series of traits is positively correlated with the trait importance, it is sufficient to conclude that the relatively more important traits in the series are under positive selection. Here, the expression level of a focal gene in different cell types can serve as such a trait series. Next, an estimate of the trait importance is needed. Gene expression noise is commonly considered to have been extensively reduced by stabilizing selection (Raj et al., 2010; Metzger et al., 2015). Specifically, it has been shown that conserved genes tend to display low transcriptional noise, i.e. stronger expression constraints (Barroso et al., 2018). Furthermore, such constraint on noise may restrain the evolvability of gene expression (Lehner, 2008). Thus, we reason that the within-cell-type expression noise can reflect the trait importance, and comparing the between-species expression divergence to the within-cell-type expression noise across cell types may reflect the mode of expression evolution for a gene. Specifically, if within a cell type or a group of cell types, a gene is under stringent regulation so that its expression noise is small, but meanwhile it exhibits large expression divergence between species or populations, then the expression of this gene likely experienced adaptive change in evolution.

Hence, in this study, given a single cell expression dataset with two species or populations, we decomposed the total expression variance into the divergence and noise for each gene in each cell type. Under this framework, we proposed two strategies, based on Negative Correlation (NC) or high Divergence-Variation Ratio (DVR), to find genes exhibiting large evolutionary divergence and small expression noise in certain cell types. The approaches were first applied to a single-cell expression dataset of the primate prefrontal cortex (PFC). We found specific genes showing the proposed divergence-noise pattern and are thus candidates of adaptive evolution in humans. Meanwhile, we also observed that the genome-wide divergence-noise patterns across all genes were consistent with a neutral mode of evolution. We reported pattern differences across cell types, suggesting some types such as the excitatory neurons were more subject to adaptive changes. Additional analyses revealed significant overlap between rapidly evolving genomic regions and the candidate genes, further supporting an adaptive scenario. Finally, to validate the applicability of our framework, we analyzed another case of naked mole-rat bone marrow. Putatively adaptive gene expression patterns were identified, in consistency with previously reported candidate cell types and functions such as myeloid cells and innate immunity.

Results

Decomposing the expression variance to probe adaptive evolution of gene expression in cell types across taxa

Given a comparative dataset of single-cell gene expression levels in two evolutionarily diverged taxa (species or populations), we characterize the expression divergence and noise of a gene in a defined cell population, i.e. cell type, by decomposing the expression variance into different components as done in Analysis of Variance (ANOVA). In the analyses, the expression levels were used as dependent variable, while the taxon assignment and sample identity were used as independent variables. Specifically, the total expression variance (sum of square, SS_{total}) was decomposed into three components: sum of square variance between taxa (SS_{sp}), sum of square variance between samples within both taxa (SS_{sam}) and sum of square variance between cells within samples across all taxa (SS_{cell_taxa}):

$$SS_{total} = SS_{sp} + SS_{sam} + SS_{cell\_taxa} \quad [1]$$

To characterize gene expression noise in one specific focal taxon, we also conducted decomposition for each taxon separately, separating the taxon-specific sum of square variance between cells within samples (SS_{cell_taxon}) from the taxon-specific sum of square variance between samples (SS'_{sam}):

$$SS_{taxon} = SS'_{sam} + SS_{cell\_taxon} \quad [2]$$

Dividing the sum of squares by corresponding degrees of freedom (DF s), we thus derived three mean square terms D_{sp} =

SS_{sp}/DF_{sp}, $D_{sam} = SS_{sam}/DF_{sam}$ and $V_{taxon} = SS_{cell\_taxon}/DF_{cell\_taxon}$. D_{sp} can be used to reflect the between-taxon expression level divergence regarding the focal cell population, while V_{taxon} can reflect the gene expression noise within the focal cell population in one specific taxon (Fig. 1A). Two strategies were designed to identify genes with large expression divergence and small noise in a cell type, which are candidates for adaptive expression evolution. In the first strategy, we normalized each term with the mean expression across the corresponding cell type in the focal taxon, deriving $D^n_{sp} = D_{sp}/Exp_{taxon}$, $D^n_{sam} = D_{sam}/Exp_{taxon}$, and $V^n_{taxon} = V_{taxon}/Exp_{taxon}$. Then the correlation between D^n_{sp} and V^n_{taxon} across all available cell types was calculated. Under neutral expectation, low V^n_{taxon} indicates high importance or strong constraints of the gene expression in the cell type, leading to low D^n_{sp} and positive $D^n_{sp} \sim V^n_{taxon}$ correlation. Significant negative correlation indicates that the gene shows higher divergence in the cell types where its expression noise is under stronger constraint, suggesting taxon-specific adaptation of the expression level in these cell types (Fig. 1B). To eliminate the possibility that the high between-taxon divergence is due to stochastic technical variation among samples, we further excluded genes with significant positive correlation between D^n_{sp} and D^n_{sam}, as well as those with significant negative correlation between D^n_{sam} and V^n_{taxon} (see Materials and Methods). This strategy is denoted as Negative Correlation (NC). Although straightforward, the significance of this NC strategy may suffer from genes with expression in only a small number of cell types. Hence in the second strategy, the ratios of D_{sp} to V_{taxon} were calculated for all (gene, cell type) pairs (hereby denoted as GC pairs) and directly compared. GC pairs with high D_{sp}/V_{taxon} ratios were considered as candidates for taxon-specific adaptation of the expression level (Fig. 1C). Meanwhile, we exclude genes with high D_{sam}/V_{taxon} ratios in order to mitigate the effects of between-sample variations (see Materials and Methods). This strategy is denoted as DVR, i.e. D_{sp}/V_{taxon} Ratio. For convenience, we denote the overall framework of *E*xpression *V*ariance *D*ecomposition as EVaDe.

EVaDe strategies identified candidate genes with potential cell-type-specific adaption in human PFC

The complex cell type composition of the brain has been a focus of recent researches by single-cell analyses. Specifically, the evolutionary specialization of primate, especially human brain is considered an adaptation through the gain of cognitive abilities. Thus, we analyzed a recent single-nucleus RNA sequencing dataset of the primate dorsolateral prefrontal cortex (dlPFC) (Ma et al., 2022), which has been associated with primate cognitive adaptation, to investigate if our proposed framework can reflect adaptive gene expression divergence in certain cell types. From the original dataset,

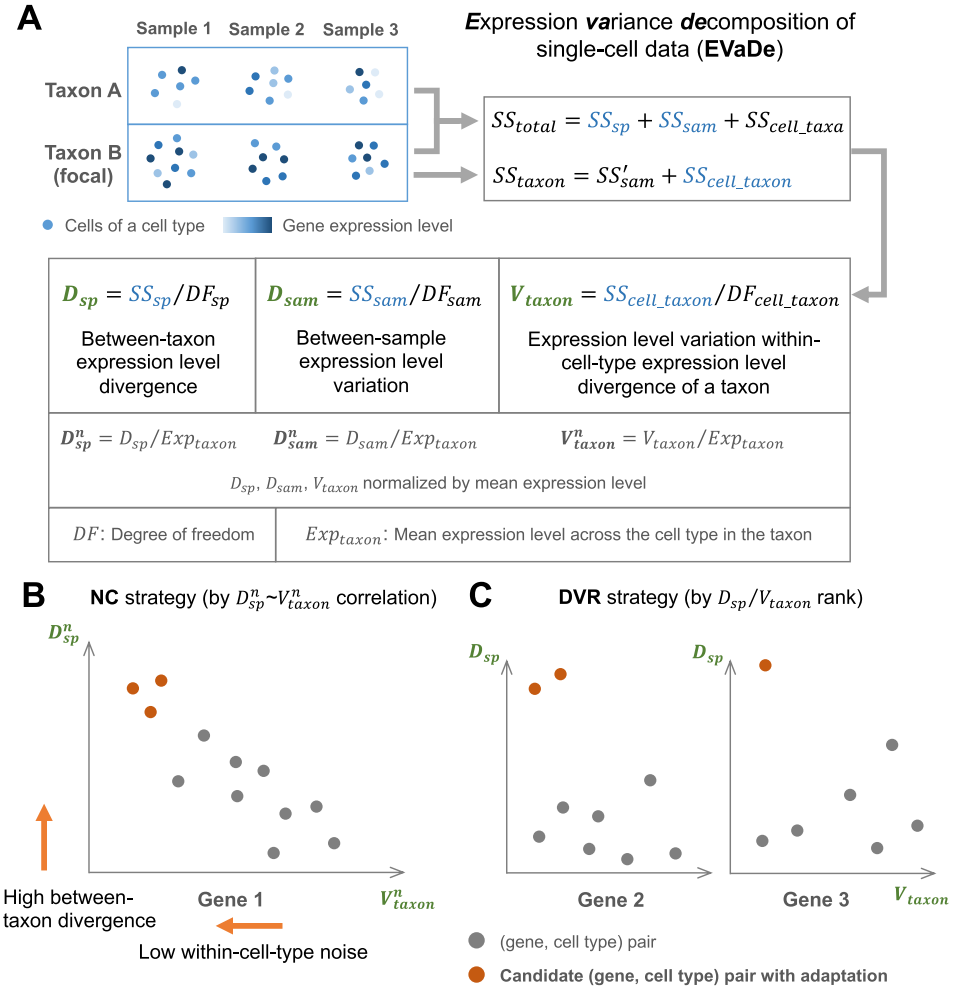

Fig. 1. Decomposing the expression variance to probe adaptive evolution of gene expression in cell types across taxa. **A**: Decomposition of single-cell expression variance. *SS* represent sum of square variances. *DF* represent corresponding degree of freedom. **B** and **C**: Two EVaDe strategies to identify genes with large expression divergence and small noise in certain cell types. NC strategy based on the negative correlation between D^n_{sp} and V^n_{taxon} across cell types (**B**). DVR strategy based on the ratio of D_{sp} to V_{taxon} (**C**).

we derived expression profiles of 28,216 genes in 45,000 cells (see Materials and Methods; Fig. S1A), previously annotated and assigned to 25 cell types existing in both human (*Homo sapiens*) and rhesus macaque (*Macaca mulatta*). By the NC strategy with human as the focal taxon, we found that 575 genes (hereby denoted key genes) showed significant $D^n_{sp} \sim V^n_{human}$ negative correlation and meanwhile showed no significant $D^n_{sam} \sim V^n_{human}$ negative correlation or positive $D^n_{sp} \sim D^n_{sam}$ correlation (significance cutoff $Q < 0.05$). In comparison, we repeated the NC analysis by using macaque as focal taxon (substituting V^n_{human} by $V^n_{macaque}$ in the analysis), and found a comparable number of 563 key genes (Figs. 2A and S1B; Table S1). Next, we conducted DVR strategy analysis with human as focal taxon. We found 393 key genes with high D_{sp}/V_{human} ratio (ranking top 0.5%) and low D_{sam}/V_{human} ratio (ranking below top 5%). Besides, DVR analysis with macaque as focal taxon obtained 283 key genes (Figs. 2A and S1C; Table S1). The intersect of human NC and DVR key genes contained 24 genes, significantly more than randomly expected ($P < 5 \times 10^{-4}$, Hypergeometric test).

To examine if the key genes are likely candidate genes for human cognitive adaptation, we then conducted functional enrichment analysis on the key genes found in the NC and the DVR analyses. Functional enrichment tests based on Gene Ontology (GO) found that the human NC key genes showed significant enrichment in terms including "fatty acid beta-oxidation" and "ncRNA processing", which are not observed in GO enrichment results of macaque NC key genes (Fig. 2B; Tables S2 and S3). Many key genes belonging to "fatty acid beta-oxidation" have previously reported associations with brain development and neuronal diseases (Heimer et al., 1993; Bryleva et al., 2010; He et al., 2011; Mizuno et al., 2013; Baloni et al., 2021; Luo et al., 2021). For example, *ACAA1* belongs to the acetyl-CoA acyltransferase family and interacts with another associated key gene *TYSND1*. It participates in the peroxisomal fatty acid β-oxidation of very-long-chain fatty acids, and its missense mutation causes early-onset Alzheimer's disease with cognitive decline (Luo et al., 2021). Correspondingly, we found that *ACAA1* exhibited a significant $D^n_{sp} \sim V^n_{human}$ negative correlation across different PFC cell types, showing low V^n_{human} and high D^n_{sp} mainly in excitatory neuron cell types such as L2–3 IT (Fig. 2C). This is also true for most other related key genes (Fig. S2A). Similarly, the role of non-coding RNA processing in cognition, brain development, and neurodegeneration has also been extensively discussed (Qureshi and Mehler, 2011; Barry, 2014; Salta and De Strooper, 2017). Examples of related key genes include the *INTS1*, *INTS10* and *ELP2*. *INTS1* and *INTS10* are subunits of the RNA polymerase II-associated Integrator complex, which is associated with transcription regulation, neural cell type differentiation and neurodevelopmental syndromes (Oegema et al., 2017; Zhang et al., 2019, 2025). *ELP2* is a core subunit of the Elongator complex that is also associated with RNA polymerase II, and its mutations lead to neurodevelopmental phenotypes such as intellectual disability (Cohen et al., 2015; Kojic et al., 2021). Both genes showed significant $D^n_{sp} \sim V^n_{human}$ negative correlation with excitatory neuron cell types displaying low V^n_{human} and high D^n_{sp}, which is also true for most other related key genes (Figs. 2D and S2B). The human key genes and the macaque key genes were identified based on the same large human-macaque expression divergence (D^n_{sp}), and both gene sets may have conserved expression noise (V^n_{human} or $V^n_{macaque}$) differences between cell types. Thus, we reasoned that the GO terms enriched in both key gene sets likely indicated genes with conserved function in the two species alongside adaptive expression divergence. These terms were mainly related to cilium organization (Table S2), and many associated key genes (e.g., *IFT172*, *CEP63*, *BBS4*, *DYNC2LI1*, *WDR19*; Figs. 2E and S2C) were components of the primary cilia, which has been shown to be essential in cortical development and neuronal differentiation (Guo et al., 2015; Youn and Han, 2018). For example, mutations in *CEP63* have been associated with developmental dyslexia and white matter volume (Einarsdottir et al., 2015). These findings suggest that the key genes with negative correlation between expression divergence and noise may have experienced adaptive evolution, contributing to human-specific cognitive functions in cell types like excitatory neurons.

The functions of human key genes found by the DVR strategy were enriched in GO terms explicitly related to brain development, specifically in axonogenesis, which are not observed in GO enrichment results for macaque DVR key genes (Fig. 2F; Tables S4 and S3). An example of key genes associated with both terms is *ROBO1*, which is regulated by another key gene *SLIT2* and participates in neocortex neuron proliferation, axon guidance, and neuron migration during development (Andrews et al., 2006; Yeh et al., 2014). Mutations in *ROBO1* and another key gene *KIAA0319* have also been associated with language and mathematics ability in developmental dyslexia (Mascheretti et al., 2014). In the DVR analysis, *ROBO1* exhibited a high D_{sp}/V_{human} ratio and low D_{sam}/V_{human} ratio in the cell type L3-5 IT-2, thus designated as a key gene (Fig. 2G). Other key genes were related to high D_{sp}/V_{human} ratio in other cell types, such as the neurodevelopmental gene *CNTN6* (Hu et al., 2015) in L3–5 IT-1, L3–5 IT-3, and L6 IT-1 (Fig. S2D). The GO enrichment results for macaque DVR key genes were largely different, but still share significant terms in the Cellular Component (CC) category such as "dendritic shaft", involving common key genes such as *NLGN1* (Table S4), whose expression in specific neuron subpopulations was known to modulate memory formation and strength (Katzman and Alberini, 2018). Among the 24 human key genes significant in both NC and DVR analyses, many were related to fatty acid metabolism, neuronal differentiation and cognitive functions (Daneshmandpour et al., 2018; Wu et al., 2024).

Various validation analyses supported the findings of the EVaDe strategies in human PFC

As a potential confounding factor, we tested the impact of gene expression, which has been associated with many genomic patterns. For example, the faster divergences at protein sequence level and expression profile level have been related to low gene expression levels (Liao and Zhang, 2006; Zhang and Yang, 2015). Are the NC and DVR key genes also of lower expression levels? To answer this question, we investigated the expression of the key genes discovered under the NC and the DVR strategies, in the respective cell types with highest D_{sp}/V_{human} ratio for each gene (see Materials and methods). We found that they were relatively highly expressed compared to all genes in their highest D_{sp}/V_{human} cell types (Fig. S3A). This supported that the expression divergences of the key genes are not due to stochastic expression drift. Interestingly, the mean expression level differences of these NC and DVR key genes between human and macaque exhibited different patterns, with the NC key genes showing higher human expression and the DVR key genes showing large variation alongside lower human expression (Fig. S3B). This suggested that the two strategies may be sensitive to different genes. Since the NC strategy requires an expression-related pattern across multiple cell types, its findings may be constrained to genes with more conserved expression and functions, and adaptation led to consistently higher expression in human than those in macaque. Furthermore, were the functional enrichment we observed in DVR analysis dominated by lowly expressed key genes? To test this possibility, we excluded genes with normalized expression level lower than 0.2, and conducted GO enrichment tests with the remaining 216 key genes in human DVR

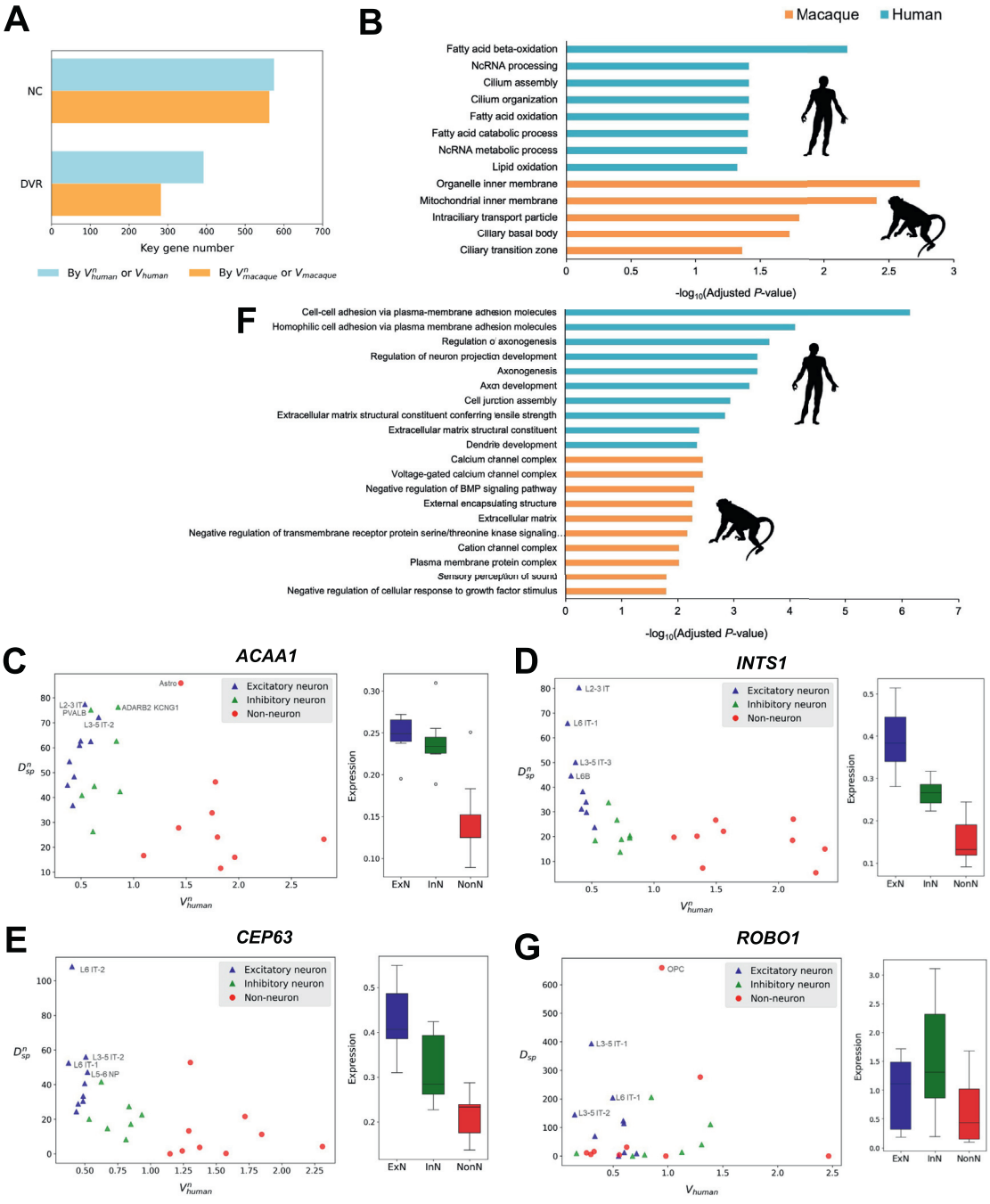

Fig. 2. EVaDe strategies identify candidate genes with potential cell-type-specific adaption in human PFC. **A**: Number of key genes identified using the NC and DVR strategies. Orange bars represent gene numbers using macaque as focal taxon, while blue bars represent gene numbers using human as focal taxon. **B**: GO enrichment analysis results of NC key genes identified in human and macaque. Terms with adjusted $P < 0.05$ are shown. **C**–**E**: Characterization of NC key genes *ACAA1* (**C**), *INTS1* (**D**), and *CEP63* (**E**). Scatter plots (left panels) display negative correlation between D^n_{sp} and V^n_{human} across different cell types. Box plots (right panels) show the distributions of mean expression levels (mean log-normalized counts across cells) for the key gene across cell types within each major cell class (excitatory neurons, inhibitory neurons, and non-neuron cells) in human. The lower and upper edges of a box represent the first (qu1) and third (qu3) quartiles, respectively, the horizontal line inside the box indicates the median (md), and the whiskers extend to the most extreme values inside inner fences, md $\pm$ 1.5 (qu3 $-$ qu1). **F**: GO enrichment analysis results of DVR key genes identified in human and macaque. The top 10 GO terms in each case are displayed in order of the adjusted *P* values. **G**: Characterization of the DVR key gene *ROBO1*, plotted in the same manner as panel (**C**–**E**). ExN, excitatory neurons; InN, inhibitory neurons; NonN, non-neuron cell types. See Materials and Methods for the full cell type names corresponding to the cell type labels in panels (**C**–**E**) and (**G**).

results and 109 key genes in macaque DVR results. These human DVR key genes were still enriched in neurodevelopment-related GO terms such as "neuron projection morphogenesis" ($Q < 0.05$, nominal $P < 2 \times 10^{-4}$), which were not observed in the GO enrichment analysis of the 109 macaque DVR key genes (nominal $P > 0.04$; Fig. S3C; Tables S5 and S3). Meanwhile, many key genes in the previous human DVR results remained as key genes after applying the expression level cutoff of 0.2, such as *ROBO2* and *FGF13*, both related to neurodevelopment and cognition (St Pourcain et al., 2014; Pan et al., 2021). To further investigate the potential impact of different background gene sets in the human and macaque GO enrichment tests, we repeated the analyses here, setting the background as the union of the two background gene sets. The results in Fig. S3C were virtually unchanged (Fig. S3D), excluding the possibility that the human versus macaque GO enrichment differences were caused by different backgrounds. Finally, to validate that between-cell-type differences in expression level do not dominate the NC test results, for two key genes *ACAA1* and *INTS1*, we normalized the expression in all available cell types to the same level as the cell type with the lowest non-zero expression, and repeated the NC tests. We found that both genes still exhibit significant D^n_{sp}-V^n_{human} negative correlations (Fig. S3E), with the cell type rankings of D^n_{sp} and V^n_{human} similar to the original patterns (Fig. 2C and 2D). Thus, our findings of the key genes held true independent of the between-cell-type gene expression level differences.

We chose to compare human and macaque for the reason that, sufficient level of expression divergence would ensure the power of adaptive pattern detection. Theoretically, human-specific expression adaptation should also be identified in more closely related species pairs. Hence, we replicated the NC and DVR analyses on 40,000 cells of human and chimpanzee (*Pan troglodytes*). Among the same 28,216 genes in 25 cell types, with human as the focal taxon, NC strategy identified 465 key genes, and DVR strategy found 282 key genes. The two sets of key genes showed significant overlap with the respective human-macaque key genes (81 and 43, $P < 1 \times 10^{-300}$, Hypergeometric test). GO enrichment tests led to few functional enrichments of the NC key genes (Fig. S3F). This is consistent with the previous indication that NC strategy was more sensitive to conserved gene expression changes, which were more challenging to detect between the much more recently diverged human and chimpanzee. In contrast, the DVR key genes exhibited enriched GO terms similar to those found among human-macaque key genes, including "neuron recognition" and "axonal fasciculation" (Fig. S3F) and involving the same key genes such as *CNTN6* (Table S6). Hence, with lower level of divergence and probably less power in reflecting adaptation, the human-chimpanzee comparison results reassuringly corroborated the initial findings in human-macaque comparison.

To compare with existing methods for gene expression adaptation, we adopted the Expression Variance and Evolution (EVE) model (Rohlfs and Nielsen, 2015) for human-macaque comparison. Since EVE was developed for tissue expression data, we pooled all cell types together and tested whether the expression of each gene showed significantly high between-species divergence based on its within-species variation (see Materials and Methods). In total, we found 958 genes with $Q < 0.05$. While these genes show certain level of overlap with the NC/DVR key genes (15% and 6%), GO enrichment analysis resulted in vastly different functional terms from those of the key genes, mainly related with cotranslational protein targeting (Fig. S3G and S3H). Thus, with cell-type-specific information, our single cell analysis framework may discover novel candidates for expression adaptation.

To validate the findings in the human-macaque comparison, we conducted three more analyses. First, we independently repeated the sampling of 45,000 cells from the original dataset, and conducted the NC and DVR analyses with human as the focal taxon to check if the results were robust to data sampling. Consequently, 555 and 403 key genes were found in the two analyses, among which 402 and 285 ($\geq$70%) overlapped respectively with the previous NC and DVR key genes. Besides, the GO enrichment analyses recapitulated the previous results, featuring cilium-related terms and axon development terms (Fig. S3I and S3J). The key gene overlap and functional enrichment of the resampled cell dataset demonstrated the robustness of the method's results against possible data heterogeneity.

Second, the cell types used in analysis may have evolutionary relatedness, rendering the correlation biased in the NC strategy. However, such relatedness is theoretically and technically hard to quantify for a standard phylogenetic regression. Technically, a tree based on expression distances effectively eliminates similarity between cell types, regardless of whether it results from evolutionary history or functionality. Theoretically, the expression differences between cell types are realized by major transitions of regulatory circuits during development, which can hardly be attributed to evolutionary contingency, but mostly result from functional adaptation. Consequently, NC analysis with phylogenetic regression by expression similarity would be over-conservative. Nonetheless, we conducted NC analysis with human as focal taxon based on Phylogenetic Least Square (PGLS, see Materials and Methods), and obtained 319 key genes, among which 288 (90.3%) also appeared in the original 575 NC key genes, including many previously mentioned key genes such as *INTS1*, *CEP63*, *IFT172*, and *BBS4*. Although GO enrichment analyses did not find significant terms with $Q < 0.05$, top-ranked terms such as "ncRNA processing" ($P < 0.0002$) exhibited nominal significance. Hence, we think the conservative NC analysis by PGLS still partially reflected the original patterns and supported our findings.

Third, as a negative control, we shuffled the sample labels randomly among all cells in each cell type, and repeated the NC and DVR analyses to exclude the possibility that the key gene assignment was artifactual due to potential biases. Consequently, we found only one NC key gene (*RP11-35L17.3*) and 1203 DVR key genes (from 1239 GC pairs). The excessive amount of DVR key genes was likely due to reduced overlap between the genes with high D_{sp}/V_{taxon} ratio and the genes with high D_{sam}/V_{taxon} ratio after random shuffling. These shuffled DVR key genes and the real DVR key genes showed no significant overlap ($P > 0.9$, Hypergeometric test), and GO enrichment analysis resulted in no significant terms. Hence, our findings of the human-macaque comparison were not the results of potential technical biases.

To summarize, the human-specific enrichment of cognition-related biological processes and these functionally related key genes indicated that the NC and DVR strategies can reflect candidate genes involved in the cell-type-specific adaptation of gene expression during human PFC evolution.

The overall pattern of divergence and noise revealed genome-wide neutral modes of expression evolution

While we observed the expression of multiple genes showed $D^n_{sp} \sim V^n_{human}$ negative correlation or high D_{sp}/V_{human} ratio, suggesting adaptation under directional selection, previous studies support an overall mode of stabilizing selection for gene expression (Rifkin et al., 2003; Hodgins-Davis et al., 2015). To validate the genome-wide evolutionary mode under our EVaDe framework, we lumped 12,639 genes expressed in all 25 cell types together and investigated the relationship between D^n_{sp} and V^n_{human} (Fig. 3A; see Materials and Methods). We found a strong positive correlation between the mean D^n_{sp}'s and the mean V^n_{human}'s across these cell types (Pearson's $r = 0.67$, Spearman's $\rho = 0.68$, both $P < 3 \times 10^{-4}$). Hence among

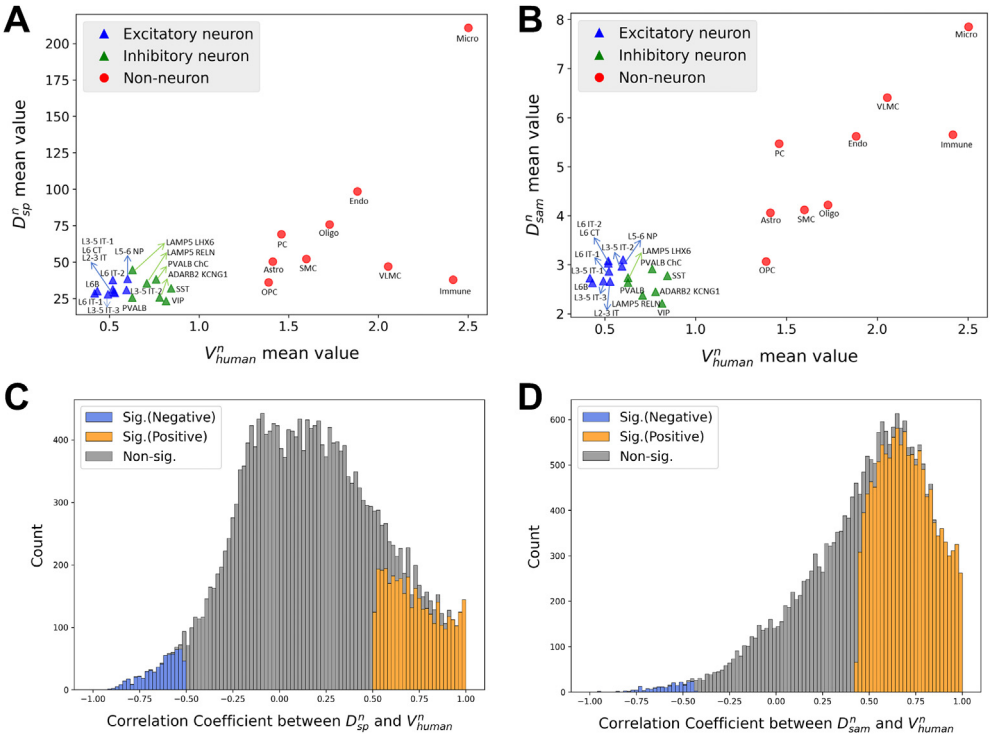

Fig. 3. The overall pattern of divergence and noise reveals genome-wide neutral modes of expression evolution. **A** and **B**: Scatter plots of (**A**) mean D^n_{sp} versus mean V^n_{human} and (**B**) mean D^n_{sam} versus mean V^n_{human} across 12,639 genes exhibiting conserved expression in all 25 cell types. Dots representing different cell types are colored according to their cell type classes (excitatory neurons, inhibitory neurons, and non-neuron cells). **C** and **D**: Histograms of Pearson correlation coefficients between (**C**) D^n_{sp} and V^n_{human} (**D**) D^n_{sam} and V^n_{human} across cell types with non-zero expression for all genes ($N = 21{,}558$). Significant negative or positive correlations ($Q < 0.05$ by Benjamini-Hochberg correction) are highlighted respectively in blue or orange. Sig., significant. Non-sig., non-significant.

genes with conserved expression across all PFC cell types, larger divergence was observed in cell types with a high expression noise, corresponding to low expression constraint. This overall pattern of expression evolution is consistent with a neutral evolution scenario under a possible level of stabilizing selection. Notably, the neuron cell types tend to show small average D^n_{sp} and V^n_{human}, especially the excitatory neurons, while the non-neuron cell types display varying patterns (Fig. 3A). The endothelial cells (Endo) and microglia cells (Micro) simultaneously showed higher D^n_{sp} and high V^n_{human} than most other cell types, while cell types such as immune cells (Immune) and vascular leptomeningeal cell (VLMC) showed low D^n_{sp} alongside with high V^n_{human}. Interestingly, when plotting the relationship between D^n_{sam} and V^n_{human} as a control, we found that the overall relationship was more heterogeneous across cell types (Pearson's $r = 0.90$, $P < 6 \times 10^{-10}$; Spearman's $\rho = 0.65$, $P < 4 \times 10^{-4}$; Fig. 3B). Relative to the pattern in Fig. 3A, the D^n_{sam} of excitatory neurons tend to be higher than those of the inhibitory neurons, and the $D^n_{sam} \sim V^n_{human}$ linearity among non-neuron cell types was stronger than that of $D^n_{sp} \sim V^n_{human}$ (Fig. 3B). Specifically, the Immune and VLMC cell types do not show low levels of D^n_{sam}. Taking the $D^n_{sam} \sim V^n_{human}$ pattern as reference, these differences indicate that regarding the genome-wide between-taxon expression divergence (D^n_{sp}) of all genes, some cell types such as the excitatory neurons, immune cells and VLMC may have undergone stronger stabilizing selection. Alternatively, we note that the Immune cell type is likely a mixture of various cell types, possessing higher heterogeneity than other cell types analyzed here. This may also contribute to the high D^n_{sam} observed. Similar to these mentioned patterns, considering all genes expressed in at least one cell type, the $D^n_{sp} \sim V^n_{human}$ trend and the $D^n_{sam} \sim V^n_{human}$ trend are also different, confirming the gene expression evolution modes found above (Fig. S4A and S4B; see Materials and methods).

To further validate the genome-wide mode, we evaluated the Pearson correlation coefficients of $D^n_{sp} \sim V^n_{human}$ and of $D^n_{sam} \sim V^n_{human}$ for each gene among cell types with non-zero expression (Fig. 3C and 3D). More genes showed significant $D^n_{sp} \sim V^n_{human}$ negative correlation (Fig. 3C) than showing significant $D^n_{sam} \sim V^n_{human}$ negative correlation (Fig. 3D), putatively corresponding to our key genes with adaptive expression evolution. Nevertheless, most genes showed positive correlations between D^n_{sam} and V^n_{human}, reflecting a baseline trend of stochastic variation among samples (Fig. 3D). Similarly, most genes showed positive or non-significant correlations between D^n_{sp} and V^n_{human}, corresponding to a neutral evolution scenario with possible stabilizing selection (Fig. 3C). The overall $D^n_{sp} \sim V^n_{human}$ correlation patterns confirmed that the expression of most genes evolve under a neutral scenario with stabilizing selection, while our putative key genes show a different mode.

The excitatory neurons displayed strong signals of adaptive expression evolution in human PFC

Single cell data enable us to shift the point of view from genes to individual cell types. Thus, which cell types have experienced more expression profile adaptation during human PFC evolution? In the above analyses, most key genes exhibited high between-taxon expression divergence and low within-cell-type expression variation in neuron cell types, especially excitatory neurons (Figs. 2 and S2). Hence indeed, distinct cell types may have evolved under different amounts of directional selection pressure on expression. To validate this difference, we first counted the number of key genes associated with each cell type in the DVR analysis. An obvious pattern is that most excitatory neuron cell types ranked higher than any of the non-neuron cell types. Cell types associated with more

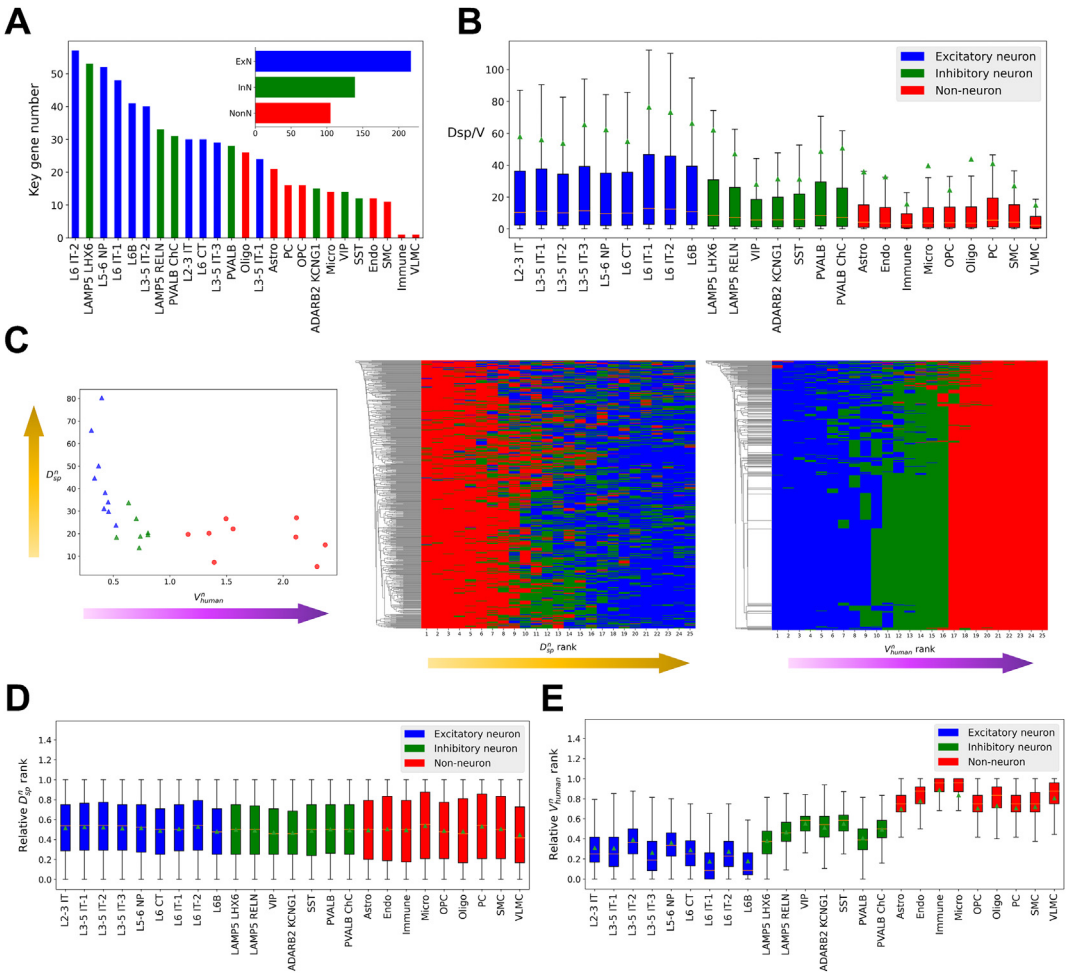

Fig. 4. The excitatory neurons displayed strong signals of adaptive expression evolution in human PFC. **A**: Bar plots of DVR key gene numbers associated with each cell type. The cell types are ranked from the largest associated key gene numbers to the smallest. The inset shows the union numbers of associated key genes across cell types in each cell type class. ExN, excitatory neurons; InN, inhibitory neurons; NonN, non-neuron cells. **B**: Box plots showing the D_{sp}/V_{human} ratio distributions of all genes with $Exp_{human} > 0.01$ in each of the 25 cell types. Green triangles indicate mean values. **C**: Cell types ranked by D^n_{sp} and V^n_{human} for each NC key gene. The left scatter plot shows D^n_{sp} versus V^n_{human} values across different cell types in the human PFC for *INTS1* as schematic example. Heatmaps display the ranking of cell types by D^n_{sp} (middle panel) and V^n_{human} (right panel). Each row corresponds to a key gene and different rows are clustered by UPGMA algorithm on Euclidean distances. **D** and **E**: Box plots summarizing the relative (**D**) D^n_{sp} and (**E**) V^n_{human} ranks of each cell type in all genes with non-zero expression. In all panels, excitatory neurons are indicated in blue, inhibitory neurons in green, and non-neuron cells in red. For panels (**B**), (**D**), and (**E**), the lower and upper edges of a box represent the first (qu1) and third (qu3) quartiles, respectively, the horizontal line inside the box indicates the median (md), and the whiskers extend to the most extreme values inside inner fences, md ± 1.5 (qu3 − qu1).

than 50 key genes include L6 IT-2, LAMP5 LHX6, and L5-6 NP (Fig. 4A). In contrast, the Immune and VLMC cell types were each associated with only one key gene, consistent with their low D^n_{sp} levels in Fig. 3A. Similarly, previous analysis by Jorstad et al. found the most human-specific DEGs in excitatory neurons and the fewest in non-neuron cell types, and they attributed this pattern to fewer expressed genes in the latter (Jorstad et al., 2023). However, the fraction of associated key genes in all expressed genes (Fig. S5) also exhibited a very similar pattern as in Fig. 4A. Next, we plotted the distribution of D_{sp}/V_{human} ratios of all genes expressed in each cell type, and again observed that the excitatory neurons showed higher ratios than those of the inhibitory neurons, which were in turn higher than the ratios of the non-neuron cell types (Fig. 4B).

In the NC analysis, for virtually all the 575 key genes we found with human as focal taxon, the ranks of D^n_{sp} across all cell types tend to be high for excitatory neurons, medial for inhibitory neurons, and low for non-neuron types. Meanwhile, the V^n_{human} ranks displayed the opposite pattern (Fig. 4C; see Materials and methods). Furthermore, across all genes, we summarized the relative D^n_{sp} and V^n_{human} ranks of each cell type among cell types with non-zero expression for each gene (see Materials and Methods). Non-neuron cell types exhibit diverging relative D^n_{sp} ranks, with microglia cells ranking the highest among all types and VLMC ranking the lowest (Fig. 4D). Nevertheless, excitatory neurons tend to have higher rankings at least compared to inhibitory neurons. The relative V^n_{human} ranking pattern across all genes resembled that of the key genes (Fig. 4E). Additionally, we note that the high D^n_{sp} and low V^n_{human} ranks of excitatory neurons in NC key genes were not solely caused by expression level differences among the three cell type classes, since not all these genes showed high excitatory neuron expression (Fig. S2A and S2B).

Overall, these observations indicate that the gene expression of excitatory neurons may have experienced more prevalent and stronger adaptive divergence, driven by directional selection, during the evolution of the human lineage (hominoids).

The key genes were associated with rapidly evolving non-coding elements (RECNEs) in human evolution

The change of gene expression during evolution most likely results from sequence changes in regulatory elements. Recently, there

have been multiple studies delimiting conserved genome regions in multiple taxa with rapid evolution in the lineages of interest (Sackton et al., 2019; Bi et al., 2023; Keough et al., 2023; Zhuang et al., 2023), demonstrating that these "accelerated regions" are associated with lineage-specific adaptation. To support our findings on expression patterns by orthogonal sequence-level signals, we extracted 1109 conserved noncoding elements with rapid evolution (RECNEs) specific to the human lineage from a comparative analysis across 52 primate species (Shao et al., 2023; Zhuang et al., 2023). Then, we searched for the nearest protein-coding genes within the 100 kb flanking regions of the RECNEs as flanking genes (see Materials and methods). Out of 14,914 background genes with normalized expression levels over 0.01 in the DVR analysis, 343 were identified as flanking genes. Among these flanking genes, 28 of them belonged to the 341 protein-coding key genes we found. By hypergeometric test, this enrichment of key genes in RECNE flanking regions is significant ($P = 6 \times 10^{-9}$; Table 1), indicating that the expression changes of the key genes are related to rapidly evolving sequences with putative regulatory significance. Among these key genes in RECNE flanking regions, there were previously discussed candidates related to neurodevelopment and cognition, such as *ROBO1/2*, *NLGN1*, and *FGF13* (Tables S4 and S5).

Apart from protein-coding key genes, we also tested separately whether non-coding key genes also showed enrichment near RECNEs. We found six non-coding genes out of 49 were located in RECNE flanking regions, significantly more than expected (Table 1). Furthermore, we excluded lowly expressed genes by requiring normalized expression level greater than 0.2 and still observed significant enrichment of key protein-coding genes near RECNE (Table 1). The insignificance of non-coding genes is probably due to their overall low expression compared to protein-coding genes. For NC analysis results, we found no enrichment of protein-coding genes, but enrichment of non-coding genes, near the RECNEs (Table 1). We also conducted the same tests on the macaque key genes, observing significant overlap between protein-coding DVR key genes and RECNE flanking regions at different expression level cutoffs ($P < 1 \times 10^{-5}$; Table S7). This is again consistent with the point that the macaque key genes were also defined on large human-macaque divergence in certain cell types, hence may be associated with human-specific RECNEs. In contrast, the DVR key genes found in the shuffling control, albeit in large numbers, were not enriched around RECNEs ($P > 0.8$; Table S7). To summarize, the putatively adaptive expression changes of the key genes found in our analysis were partially supported by their significant association with rapidly evolving genome regions nearby.

Case study of the EVaDe analysis on naked mole-rat found key genes related to lineage-specific immune adaptation

To validate our decomposition framework for investigating adaptive gene expression change, we conducted another case study on a comparative single cell expression dataset of the naked mole-rat (*Heterocephalus glaber*, hereby denoted as NMR) and the mouse (Lin et al., 2024). The NMR has been known and extensively studied for its prolonged lifespan, resistance to cancer and lack of age-associated mortality increase, attributed to their specialized immune system compositions and functions (Hilton et al., 2019; Lin et al., 2024). Hence in the NMR-mouse scRNA-Seq dataset, we extracted expression levels of 15,168 genes in 30,000 bone marrow cells belonging to 10 major cell types based on cell abundance. These included 9000 lymphoid lineage cells (B cell, immature B cell, pre-T cell), 15,000 myeloid lineage cells (promyelocyte, myelocyte, metamyelocyte, neutrophil, monocyte), and 6000 erythroid lineage cells (erythroid and red blood cell, i.e. RBC). We then applied the NC and DVR analyses comparing NMR and the mouse, with NMR as the focal taxon. In NC analysis, we identified six key genes exhibiting significant D^n_{sp}-V^n_{NMR} negative correlations across 10 cell types: *1810065E05Rik*, *Zdhhc12*, *Pfdn6*, *Trappc4*, *Gng10*, and *Arhgef11*. Notably, the functions of these genes are associated with immune responses to bacteria or cancer. For instance, *1810065E05Rik*, which displayed the highest D^n_{sp} and lowest V^n_{NMR} in myelocytes (Fig. 5A), has been shown to experience significant expression increase in response to intestinal *Lactobacillus* introduction or bladder *Gardnerella* exposure in mice (Archambaud et al., 2012; Gilbert et al., 2022). Moreover, *Trappc4*, also displaying high D^n_{sp} and low V^n_{NMR} in myelocytes (Fig. 5B), regulates the intracellular localization and expression of PD-1 ligand 1 (PD-L1), thus affecting anti-tumor immunity (Ren et al., 2021). Additionally, the function of *Zdhhc12*, *Gng10*, and *Arhgef11* has also been associated with cancer progression (Cardenas-Navia et al., 2010; Du et al., 2020; Lu et al., 2022).

Using the DVR method, we identified 174 GC pairs in the NMR, involving 126 key genes. GO functional enrichment analysis on these genes revealed significant enrichment in immunity-related biological processes such as "Neutrophil mediated immunity" and "Myeloid cell activation involved in immune response" (Fig. 5C; Table S7). To further explore the extent of adaptive expression evolution in different cell types of the NMR, we counted the frequency of each cell type appearing in the 174 GC pairs (Fig. 5D). The results showed that myeloid lineage cells contained the most DVR key genes (74.71% of all key genes), while lymphoid lineage cells and erythroid lineage cells were associated with much fewer key genes (respectively 15.52% and 9.77%). Among myeloid lineage cell types, myelocytes and monocytes contained the most key genes (respectively 45 and 35). Myeloid lineage cells play a major role in innate immune responses, with myelocyte being precursors to neutrophils and monocytes being precursors to macrophages and dendritic cells, all of which are important components of the innate immune system (Auffray et al., 2009; Xie et al., 2020). Thus, our findings suggested a crucial role of myeloid lineage cells in the adaptation of the NMR immune system. A previous study has found significant differences in the cellular compositions of the immune system between NMR and mice, characterized by a predominance of myeloid lineage cells and unique myeloid lineage cell types in NMR, in contrast with the dominance of the lymphocyte lineage observed in mice (Hilton et al., 2019). They proposed that the NMR immune system relies heavily on myeloid lineage cell-mediated innate immunity, consistent with the indication of our findings. Moreover, reports have indicated that NMR is highly susceptible to viral infections (Ross-Gillespie et al., 2007; Artwohl

Table 1
Coincidence of key genes near rapidly evolving non-coding elements (RECNEs) in human evolution.

Analysis	Gene type	Background	RECNE flanking genes	Key genes	Flanking key genes	*P*-value
DVR (Exp. > 0.01)	Protein-coding	14,914	343	341	28	6×10^{-9}
DVR (Exp. > 0.01)	Non-coding	3973	140	49	6	0.007
DVR (Exp. > 0.2)	Protein-coding	8700	269	190	19	6×10^{-6}
DVR (Exp. > 0.2)	Non-coding	679	58	25	2	0.65
NC	Protein-coding	16,432	366	508	8	0.88
NC	Non-coding	7956	219	64	5	0.03

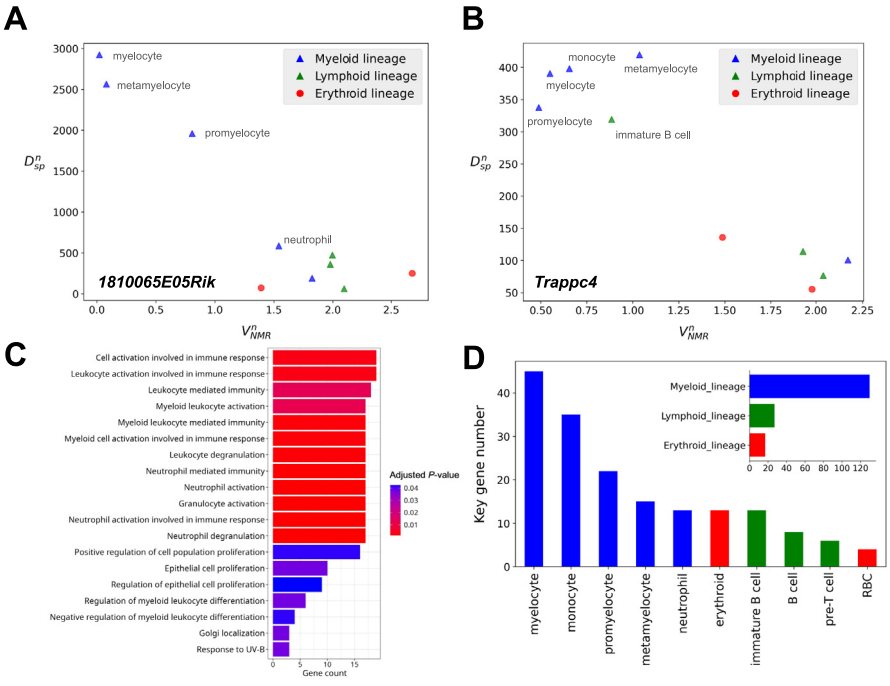

Fig. 5. EVaDe analysis on naked mole-rat indicated key genes and cell types related to lineage-specific immune adaptation. **A** and **B**: Scatter plots displaying negative correlation between D^n_{sp} and V^n_{NMR} across different cell types within the myeloid (blue), lymphoid (green), and erythroid (red) lineages for *1810065E05Rik* (**A**) and *Trappc4* (**B**). **C**: GO enrichment analysis of DVR key genes ($N = 126$) identified with NMR as focal taxon. Terms with adjusted $P < 0.05$ are shown. **D**: Bar plots of DVR key gene numbers associated with each cell type. The cell types are ranked from the largest associated key gene numbers to the smallest. The inset shows the union numbers of associated key genes across cell types in each cell type lineage.

et al., 2009), suggesting that the NMR immune system has evolved under stronger antibacterial than antiviral selective pressures (Hilton et al., 2019). Lymphoid lineage cells play a central role in adaptive immune responses and are the key force in antiviral-specific immune responses. The relatively weaker antiviral response of NMR is thus consistent with our finding that the lymphoid lineage contains fewer key genes than the myeloid lineage. This pattern further suggested a unique evolutionary path in the immune strategy of NMR, with weaker selection on antiviral functions than in mouse, possibly resulting from distinct selection pressures cast by different compositions of pathogens in subterranean environment.

Discussion

In this study, we adopted an analysis framework to explore possible adaptive evolution of gene expression in single cell expression data. Specifically, after expression variance decomposition (EVaDe) of a gene, large between-taxon expression divergence and small within-cell-type expression noise were proposed as an indication of adaptive expression change (DVR strategy). Alternatively, negative correlation between divergence and noise also looked for the same signal, but focusing on more conserved trends across multiple cell types (NC strategy). We first found hundreds of candidate genes in primate PFC showing such divergence-noise patterns. Functional enrichment analyses and literature research suggested that these key genes may contribute to the adaptive evolution of human cognition. We then reported an overall pattern of positive divergence-noise correlation for most genes, consistent with a genome-wide neutral evolution scenario under stabilizing constraints for gene expression. At the cell-type level, most key genes displayed large divergence and low levels of noise mostly in excitatory neurons, indicating these cell types may have experienced more adaptation during human PFC evolution than other types such as the non-neurons. Furthermore, it is observed that the key genes coincided with previously annotated rapidly evolving conserved noncoding elements (RECNEs) in human, orthogonally supporting their possible adaptation. Finally, the EVaDe framework was applied to another case study of naked mole-rat bone marrow. Comparing with mouse, we found candidate genes and myeloid cell types showing adaptive patterns, consistent with existing evidence of strong innate immunity in NMR.

In the case studies of both primate PFC and NMR bone marrow, we observed that the NC strategy and the DVR strategy yield different results. The NC strategy explicitly considers the expression statistics (D^n_{sp} and V^n_{taxon}) of the same gene across different cell types as a series of related traits, and directly probes the correlation between trait divergence and within-taxon trait constraint level. Hence by requiring that the gene exhibits conserved non-zero expression in multiple cell types, the NC strategy provides a valid statistical test for putative adaptation. In this sense, the NC test is relatively conservative, in that not all positive selection leads to such a negative correlation. Indeed, we observed that the GO terms found by NC referred to more generic and conserved (yet intriguingly related) functions in primate PFC, while only six NC key genes were found in the NMR case. That NC key genes are required to have conserved expression in multiple cell types of two taxa may also explain why the NC key genes did not significantly overlap with the RECNEs specific to human evolution in the primate PFC case, because the regulatory sequence change may happen earlier, not captured in the RECNE detection. In contrast, the DVR strategy focuses on individual (gene, cell type) pairs, allowing cell-type-specific genes to stand out given a high divergence-noise ratio (D_{sp}/V_{taxon}), even if the gene is only

expressed in one or two cell types. This explains why we observed neuron-specific GO terms in primate PFC and myeloid-lineage-specific GO terms in NMR bone marrow, associated with respective DVR key genes. Biologically, NC key genes not found in DVR are likely genes with more constrained and conserved expression, thus the between-taxon divergence may not be among the largest across all genes; DVR key genes not found in NC are likely less conserved, highly diverged genes specifically expressed in a small number of cell types. A gene found by both NC and DVR would have conserved expression as well as exhibiting substantially large between-taxon divergence. Technically, the power of the NC strategy correlation test is naturally bounded by the number of available cell types, which explains why many key genes were found in the primate PFC case (maximally 25 cell types) and much fewer were identified in the NMR bone marrow case (maximally 10 cell types). Thus, the NC strategy and the DVR strategy are to some extent different in terms of candidate gene expression scenarios, and may be simultaneously applied to achieve a more comprehensive characterization of putatively adaptive expression evolution.

Existing studies have tackled the task of probing evolution modes in comparative single cell datasets. However, usage of empirical statistics lacks theoretical justification and is subject to technical inaccuracy. The previous study by Ma et al. in primate PFC used Pearson correlations to reflect the expression divergence between species, and an entropy measurement to reflect expression variability within a cell population (Ma et al., 2022). A recent study in primate cerebral cortex used Spearman correlation for between-species divergence, and average between-individual correlation for expression variability (Jorstad et al., 2023). Both studies found that the non-neuron cell types exhibited the largest between-species expression divergence. However, this may be partially caused by large expression variability in these cell types as mentioned in the original text (Ma et al., 2022; Jorstad et al., 2023), and hence cannot serve as a clear support for adaptive evolution. On the other hand, differential expression analyses between human and macaque found more than a thousand differentially expressed genes (DEGs) in many individual cell types, and non-neurons have the fewest DEGs compared to neurons, especially excitatory neurons (Jorstad et al., 2023). Notably, although the human-specific DEGs were enriched in functional terms such as synapse assembly (Jorstad et al., 2023), it is unlikely that most of the more than a thousand genes experienced directional selection during adaptation. Hence, DEG analysis may not provide definitive evidence for adaptive expression change. In comparison, our EVaDe framework considers the expression of a gene in different cell types as related trait series, explicitly separate expression noises from between-taxon divergence, and tests for specific D_{sp}-V_{taxon} patterns across cell types, theoretically driven by adaptive process. We found tens of key genes associated with each cell type instead of hundreds. Moreover, our findings that excitatory neurons, especially the deep layer types (e.g. L6 IT-1) were associated with more key genes and higher D_{sp}/V_{human} ratios are consistent with the previous DEG results (Jorstad et al., 2023).

Although the EVaDe framework seems analogous to the conventional between- vs. within-species variation comparison, it is essentially different. The within-species expression variation among individuals should be mainly attributed to neutral genetic variation, so that it is previously compared to the expression divergence between species, reflecting whether the possibly neutral genetic variation can explain this divergence. The assumption in these previous studies has been yet challenged when there is non-neutral within-species divergence in structured populations. In contrast, instead of using the within-species expression variation as a reflection of the genetic variation level, we derive the within-cell-type expression variation as an estimate of the gene expression noise. This noise estimation reflects the importance or biological constraints cast on the traits, i.e. the expression of the gene in corresponding cell types, by the previously mentioned prevalent stabilizing selection. No genetic variation between cells is necessarily invoked in the assumption of this logic. Hence, the EVaDe framework is theoretically different from the conventional between-versus within-species variation comparison. The between-cell variation in the single-cell expression data can be subject to technical noise, rendering the noise comparison between genes difficult. However, single-cell expression data were previously used for gene expression noise analyses (Sun and Zhang, 2020). In addition, we note that in the EVaDe framework, the between-cell expression variation was compared between cell types for the same gene (NC strategy), or first used to calculate the D_{sp}/V_{taxon} ratio before cross-gene comparison (DVR strategy). This should diminish the impact of gene-specific technical noise in single-cell RNA sequencing. Besides, shuffling control results validated the power of our analysis on the real data. Another possible test under the EVaDe framework is to conduct F test for the D_{sp}/V_{taxon} ratios, similar to the ANOVA test. However, although providing statistical significance, F test may only describe the observation of significant expression divergence between species, but were not to pick up the top key genes under adaptation. Thus, F test may result in thousands of significant genes in each cell type analogous to the DEG analysis in previous studies. In this sense, we decided not to rely on the F test in our DVR analysis.

The analyses of evolution modes for gene expression as a phenotype have suffered from technical biases and lack of theoretical models. Single cell expression data provide the opportunity to overcome the composition biases across different taxa. However, comparative single cell datasets are also subject to analysis difficulties such as cross-species integration and cell type annotation (Price et al., 2022). In our analysis, we used the expression profile matrices and cell type assignments of the original studies, circumventing the problems assuming the published annotations are correct. It is possible that different data integration pipelines or different cell clustering resolutions may affect the EVaDe results. Although we have shown that the analysis results are largely consistent under different expression level cutoffs, further validation may provide more information about the potential impact of technical details on the results. Besides, we reckon that the current EVaDe framework serves mostly as a proof of concept, demonstrating the feasibility of applying evolutionary framework to single cell expression data. The detailed parameters in the analyses may well benefit from case-specific adjustment, such as the arbitrary rank cutoff of D_{sp}/V_{human} ratio and D_{sam}/V_{human} ratio in the DVR strategy. Furthermore, our framework is currently proposed for comparison between a pair of taxa, with the potential to be extended to multiple taxa in a phylogeny. To realize this extension, existing phylogeny-aware models of expression changes need to be integrated (Yang et al., 2019; Bertram et al., 2023). As applications of single cell RNA sequencing have been accumulating rapidly in comparative studies of non-model organisms, it would be of increasing importance to consolidate a valid analysis framework of evolution modes for such types of data.

Materials and methods

Single cell data acquisition and preprocessing

Single-cell RNA-seq data for human and macaque prefrontal cortex (PFC) were obtained as a preprocessed Seurat object from the online data of a published study (Ma et al., 2022) (https://sestanlab-public-data.s3.amazonaws.com/Primate_PFC_Ma_2022/PFC_snRNAseq_liftover.zip). The dataset comprised four human samples and four macaque samples, with 29 orthologous cell types and 28,216 orthologous genes annotated. Gene expression counts within each cell were then normalized using the NormalizeData function (scaling factor = 10,000) in the R package Seurat (version 4.1.1) (Hao

et al., 2021). To ensure sufficient representation of each cell type, we set a cell count threshold of 1800 cells per type. Cell types with fewer than 1800 cells were removed, and for the remaining cell types, 1800 cells were randomly sampled. We down-sampled to an equal number of cells for each defined cell type to avoid biases due to varying cell counts. The cell number threshold 1800 was chosen considering a trade-off between reserving more cell types for downstream analyses and retaining more cells for each type after down-sampling, as all four removed cell types contained less than 650 cells. This resulted in a final dataset of 45,000 cells across 25 cell types, including Layer 2−3 intratelencephalic (L2−3 IT), Layer 3−5 intratelencephalic 1 (L3−5 IT-1), Layer 3−5 intratelencephalic 2 (L3−5 IT-2), Layer 3−5 intratelencephalic 3 (L3−5 IT-3), Layer 5−6 near-projecting (L5−6 NP), Layer 6 corticothalamic (L6 CT), Layer 6 intratelencephalic 1 (L6 IT-1), Layer 6 intratelencephalic 2 (L6 IT-2), Layer 6B (L6B), LAMP5 LHX6, LAMP5 RELN, VIP, ADARB2 KCNG1, SST, PVALB, PVALB chandelier cell (PVALB ChC), astrocyte (Astro), microglia (Micro), oligodendrocyte (Oligo), oligodendrocyte precursor cell (OPC), endothelial cell (Endo), immune cell (Immune), pericyte (PC), smooth muscle cells (SMC), vascular leptomeningeal cells (VLMC). Cell type names without brackets were assigned according to the marker genes in the original study. In the human versus chimpanzee analysis, we followed the same data preprocessing steps, obtaining 40,000 cells belonging to 25 cell types, i.e., 1600 cells per type, for downstream analyses.

Single-cell RNA-seq data for NMR and mouse bone marrow were obtained from Gene Expression Omnibus (GEO), under accession code GSE214390 (Lin et al., 2024). The NMR dataset contained 19 cell types across four samples, each with two technical replicates, totaling 51,708 genes annotated with Ensembl or Entrez Gene IDs. The mouse dataset included 16 cell types across four samples, also with two technical replicates per sample, containing 49,671 genes annotated by Ensembl gene IDs. A Seurat object was constructed for each replicate by reading the original data files (matrix.mtx.gz, barcodes.tsv.gz, genes.tsv.gz). To assess the reproducibility of technical replicates, principal component analysis (PCA) and Uniform Manifold Approximation and Projection (UMAP) of the gene expression matrix were performed using Seurat (version 4.1.1) simultaneously on a matrix merging the two replicates of each sample. We visually inspected the UMAP visualizations to confirm that cells from the two replicates of each sample clearly clustered by cell types and overlapped within each cell cluster, thus containing little technical bias. Hence, we combined all cells from the two technical replicates for each sample into a single dataset. Orthologous genes between NMR and mouse ($N = 15{,}168$) were identified by integrating a previously established ortholog list (Hilton et al., 2019) and cross-referencing between Ensembl and Entrez Gene IDs, followed by further gene symbol mapping. Gene expression counts within each cell were normalized using the NormalizeData function (scaling factor = 10,000) in Seurat. Focusing on shared cell types between the two species and applying a cell number threshold of 3000 per cell type, 10 cell types were retained for downstream analyses, resulting in a total of 30,000 cells.

ANOVA analysis to decompose the expression variance

We decomposed the expression variance into different components to quantify gene expression divergence and noise between two evolutionarily diverged taxa (species or populations) at the single-cell level as follows. We started from the preprocessed single-cell gene expression matrix merged from those of the two individual taxa, and labeled each cell with its respective taxon and sample origin. Then, a two-way Analysis of Variance (ANOVA) by the aov(.) function in R (version 4.1.3) was conducted using the following model.

Gene Expression ~ Taxon + Sample (nested within Taxon)

Here, the normalized gene expression levels served as the dependent variable. Taxon (e.g., human or macaque) was the first independent variable, while Sample, nested within Taxon, served as the second independent variable to account for gene expression variation due to differences between individual samples within the same taxon. We extracted the Mean Square (MS) values from the ANOVA output as the metric for assessing the magnitude of expression variation attributed to different levels. The MS normalizes the sum of squares by the degrees of freedom, providing a variance estimate that is adjusted for sample sizes and is thus more comparable across datasets. Consequently, we derived the variance of gene expression across cells into inter-taxon divergence (D_{sp}), inter-sample variation within taxon (D_{sam}), and the residuals (among-cell variance within samples, V_{taxa}). To specifically characterize gene expression noise within the focal taxon, we performed a separate one-way ANOVA for each taxon using the following model:

Gene Expression ~ Sample

The normalized gene expression level served as the dependent variable and the Sample labels served as the independent variable. This allowed us to isolate the inter-sample variation within the focal taxon (D'_{sam}) and the residual cell-to-cell variance within the focal taxon (V_{taxon}).

The NC strategy

For each gene within each cell population (hereby denoted a cell type), we obtained the D_{sp}, D_{sam}, and V_{taxon} values as described above. These values were then normalized by the mean expression level (mean log-normalized counts across cells, Exp_{taxon}) of the corresponding gene within the focal taxon's cell type: $D^n_{sp} = D_{sp}/Exp_{taxon}$, $D^n_{sam} = D_{sam}/Exp_{taxon}$, and $V^n_{taxon} = V_{taxon}/Exp_{taxon}$. Genes with non-zero D_{sp}, V_{taxon}, and Exp_{taxon} values in at least five cell types were retained for downstream analyses, to ensure reasonable statistical power on correlation tests. For these genes, we performed linear regression analysis using the stats.linregress function in the scipy Python package on the D^n_{sp}, D^n_{sam}, and V^n_{taxon} values across the relevant cell types. This yielded three Pearson correlation coefficients (r values) and associated P values for each of the following pairs: $D^n_{sp} \sim V^n_{taxon}$, $D^n_{sp} \sim D^n_{sam}$, and $D^n_{sam} \sim V^n_{taxon}$. P values were further adjusted as Q values using the Benjamini-Hochberg method for multiple test correction. We first selected genes that showed a significant negative $D^n_{sp} \sim V^n_{taxon}$ correlation ($Q < 0.05$). To reduce the probability that the negative $D^n_{sp} \sim V^n_{taxon}$ correlation is stochastic with no biological significance, we further excluded genes with significant positive $D^n_{sp} \sim D^n_{sam}$ correlation ($Q < 0.05$) and genes with significant negative $D^n_{sam} \sim V^n_{taxon}$ correlation ($Q < 0.05$). The remaining genes were denoted as NC key genes.

The DVR strategy

In the DVR strategy, we looked for putatively adaptive gene expression patterns in specific cell types, hence focusing on (gene, cell type) pairs, or GC pairs. GC pairs with extremely low mean expression level ($Exp_{taxon} < 0.01$) and GC pairs with zero D_{sp} or V_{taxon} values were excluded, to enable D_{sp}/V_{taxon} ratio calculation and avoid stochastic outlier values with no biological significance. For the remaining pairs, we calculated the ratios of D_{sp} to V_{taxon} and D_{sam} to V_{taxon}. Based on these two ratios, the cell type pairs are then ranked from highest to lowest respectively. To identify GC pairs with high between-taxon expression divergence and low within-cell-type noise, while minimizing the impact of stochasticity reflected by between-sample variance, we employed a two-step selection process. First, a specific threshold is set to select GC pairs with a high D_{sp}/V_{taxon} rank. Then, a second threshold was applied to filter out

GC pairs with a high D_{sam}/V_{taxon} rank. The remaining GC pairs were denoted as DVR key GC pairs, and genes involved in these GC pairs were denoted as DVR key genes. Specifically, for the human-macaque PFC case, we empirically selected GC pairs whose D_{sp}/V_{taxon} rank was in the top 0.5%, and simultaneously required the D_{sam}/V_{taxon} rank was not in the top 5%. For the NMR-mouse bone marrow case, we selected GC pairs whose D_{sp}/V_{taxon} rank was in the top 1%, and simultaneously required the D_{sam}/V_{taxon} rank was not in the top 5%. These percentage cutoffs were set to maintain a reasonable number of top-ranked genes for downstream functional enrichment analysis.

Gene Ontology (GO) enrichment analysis

GO enrichment analysis was performed using the enrichGO function in the R package "clusterProfiler" (version 4.0.5) (Yu et al., 2012). Different background gene sets were used depending on the specific analysis scenarios. For the NC method, the background gene set contained all genes with non-zero D_{sp}, V_{taxon}, and Exp_{taxon} values in at least five cell types. For the DVR method, the background gene set consisted of genes with Exp_{taxon} above 0.01 (or 0.2 when explicitly mentioned in the main text), and with non-zero D_{sp} and V_{taxon} values in at least one cell type. The Benjamini-Hochberg method was used to control the false discovery rate (FDR), and a Q value < 0.05 was considered statistically significant.

Validation analyses for the human PFC findings

For key GC pairs identified by the DVR strategy, the expression levels of each gene within its corresponding cell types were obtained to represent DVR gene expression levels in Fig. S3A and S3B. For each key gene identified by the NC method, the D_{sp}/V_{taxon} ratios were calculated across all cell types with $Exp_{taxon} > 0.01$. The cell type with the maximum ratio was selected, and the mean expression within that cell type was obtained for the key gene. These expression levels were then collected for all NC key genes to represent NC gene expression levels in Fig. S3A and S3B. For comparison, the expression levels of all genes were also evaluated. For each gene, the D_{sp}/V_{taxon} ratios were calculated across all cell types with $Exp_{taxon} > 0.01$. The cell type with the maximum ratio was selected, and the mean expression within that cell type was obtained for the gene. These expression levels were then collected for all genes to represent all gene expression levels in Fig. S3A and S3B. Pairwise t-tests were performed between NC genes, DVR genes, and all genes using the Python function "scipy.stats.ttest_ind".

The cutoff of 0.2 for defining genes with high expression level was set arbitrarily to exclude relatively lowly expressed genes potentially with larger stochastic expression divergence or noise.

For the EVE model analysis, we first pooled the expression levels across all 45,000 cells together, did normalization as described above, and then conducted the betaSharedTest in the R package evemodel (https://gitlab.com/sandve-lab/evemodel/). Likelihood ratio test P values were derived according to the output likelihood ratio statistics.

For the PGLS analysis, we first calculated the mean expression level of each gene in each cell type, and then derived a correlation distance matrix by calculating one minus the expression profile Pearson correlation between all pairs of cell types. The distance matrix was used to reconstruct a Neighbor-Joining tree of the cell types, based on the as.phylo function in the R package APE v5.8-1 (Paradis and Schliep, 2019). Next, PGLS was conducted by the R package caper v1.0.3. The key genes were identified as those showing significant negative $D^n_{sp} \sim V^n_{taxon}$ regression coefficient ($Q < 0.05$) with no significant positive $D^n_{sp} \sim D^n_{sam}$ regression coefficient and no significant negative $D^n_{sam} \sim V^n_{taxon}$ regression coefficient ($Q < 0.05$).

For the shuffling control, we shuffled the sample labels randomly among all cells in each cell type, so that each sample after shuffling contained the same number of cells as in the real data. The NC and DVR analyses were then conducted.

Genome-wide analysis of D^n_{sp}-V^n_{taxon} and D^n_{sam}-V^n_{taxon} correlations in human PFC

For each cell type, the mean D^n_{sp} was calculated by summing the D^n_{sp} for each analyzed gene and dividing the sum by the number of expressed genes ($Exp_{human} > 0$) within that cell type. Mean D^n_{sam} and mean V^n_{human} were calculated likewise. Spearman and Pearson correlation coefficients were computed using the spearmanr and pearsonr functions, respectively, from the "scipy.stats" module in Python.

Two sets of genes were analyzed. The first set consisted of 12,639 genes exhibiting conserved expression across all PFC cell types, defined as showing $Exp_{human} > 0$ in all 25 cell types. This set was used in Fig. 3. The second set comprised 25,073 genes expressed in at least one cell type, defined as having $Exp_{human} > 0$ in any of the 25 cell types. This set was used in Fig. S4.

Cell types ranking by D^n_{sp} or V^n_{human} in human PFC

For each key gene identified by the NC method, the 25 cell types were ranked based on their D^n_{sp} values in ascending order. Cell types with missing D^n_{sp} values were assigned 0. The ranked cell types were then assigned values of '0′, '1′, or '2′ corresponding to their classification as excitatory neurons (ExN), inhibitory neurons (InN), or non-neuron cells, respectively. Heatmaps in Fig. 4C were generated using Seaborn (version 0.11.2) (Waskom, 2021), with rows clustered. A separate heatmap was generated for the 25 cell types ranked according to their V^n_{human} values, also in ascending order. Cell types with missing V^n_{human} values were assigned the value 100,000. Across all 25 cell types $\times$ 575 key genes in Fig. 4C, there were only 30 missing values in 23 genes, causing little impact on the figure patterns.

For each gene in the genome, cell types with $Exp_{human} > 0$ were selected. If the number of such cell types n was greater than five, these cell types were ranked according to their D^n_{sp} values. The rank indices were normalized by dividing the actual rank value by n-1, deriving the final relative D^n_{sp} ranks of each cell type. For each of the 25 cell types, the relative D^n_{sp} rank values of all genes within the cell type were aggregated to form the box plots in Fig. 4D, using the Python module "matplotlib.pyplot". The same procedure was applied to generate box plots of relative V^n_{human} rank values in Fig. 4E.

Nearest genes to human rapidly evolving non-coding elements (RECNEs)

To obtain the nearest genes to human RECNEs, we first downloaded the genome position data of RECNEs from a previous study (Shao et al., 2023), which was based on the human genome reference annotation (*Homo sapiens* hg38, Ensembl v100). Next, we retrieved the coding sequence (CDS) position information for all protein-coding genes and gene position information for all lncRNA genes from the Ensembl v100 annotations. Then, using the bedtools (version 2.30.0) intersect command (Quinlan and Hall, 2010), we searched for the protein-coding genes and lncRNA genes within a 100 kb window upstream and downstream of each RECNE, and identified the nearest ones by in-house script. Subsequently, we converted the annotations of these nearest genes using the GTF

format annotation file for GENCODE human genome v28, and identified intersections between these nearest protein-coding or lncRNA genes and the key genes found in EVaDe analyses. A hypergeometric test (Python scipy.stats module) was used to assess the significance of the intersections.

Data and code availability

All data sources needed to evaluate the conclusions in the paper are present in the paper and the Supplementary Materials. Source codes for all essential analyses are available at https://github.com/qin-proj/EVaDe. The initial expression matrices and other essential data are available at https://figshare.com/s/5ea408815fa30b2764e1. Additional data and scripts related to this paper may be requested from the authors.

CRediT authorship contribution statement

Tian Qin: Conceptualization, Methodology, Software, Formal analysis, Writing - Original Draft, Visualization. **Hongjiu Zhang**: Methodology, Writing - Review & Editing. **Zhengting Zou**: Conceptualization, Methodology, Writing - Review & Editing, Supervision.

Conflict of interest

The authors declare no conflict of interest.

Acknowledgments

We thank Dr. Jianzhi Zhang, Dr. Wenfeng Qian, Dr. Weiwei Zhai, Lin Chen, Han Liu, Jianwei Mao and anonymous reviewers for valuable comments. This work was supported by the National Natural Science Foundation of China, and institutional grants to Z.Z from the State Key Laboratory of Animal Biodiversity Conservation and Integrated Pest Management, Institute of Zoology, Chinese Academy of Sciences and the Institute of Zoology, Chinese Academy of Sciences.

Supplementary data

Supplementary data to this article can be found online at https://doi.org/10.1016/j.jgg.2025.04.022.

References

Andrews, W., Liapi, A., Plachez, C., Camurri, L., Zhang, J., Mori, S., Murakami, F., Parnavelas, J.G., Sundaresan, V., Richards, L.J., 2006. Robo1 regulates the development of major axon tracts and interneuron migration in the forebrain. Development 133, 2243–2252.

Archambaud, C., Nahori, M.A., Soubigou, G., Becavin, C., Laval, L., Lechat, P., Smokvina, T., Langella, P., Lecuit, M., Cossart, P., 2012. Impact of lactobacilli on orally acquired listeriosis. Proc. Natl. Acad. Sci. U. S. A. 109, 16684–16689.

Artwohl, J., Ball-Kell, S., Valyi-Nagy, T., Wilson, S.P., Lu, Y., Park, T.J., 2009. Extreme susceptibility of African naked mole rats (*Heterocephalus glaber*) to experimental infection with herpes simplex virus type 1. Comp. Med. 59, 83–90.

Auffray, C., Sieweke, M.H., Geissmann, F., 2009. Blood monocytes: development, heterogeneity, and relationship with dendritic cells. Annu. Rev. Immunol. 27, 669–692.

Bakken, T.E., Jorstad, N.L., Hu, Q., Lake, B.B., Tian, W., Kalmbach, B.E., Crow, M., Hodge, R.D., Krienen, F.M., Sorensen, S.A., et al., 2021. Comparative cellular analysis of motor cortex in human, marmoset and mouse. Nature 598, 111–119.

Baloni, P., Nho, K., Arnold, M., Louie, G., Kueider-Paisley, A., Saykin, A.J., Ekroos, K., Funk, C., Hood, L., Price, N.D., et al., 2021. Investigating the importance of acylcarnitines in Alzheimer's disease. Alzheimer's Dement. 17, e056647.

Barroso, G.V., Puzovic, N., Dutheil, J.Y., 2018. The evolution of gene-specific transcriptional noise is driven by selection at the pathway level. Genetics 208, 173–189.

Barry, G., 2014. Integrating the roles of long and small non-coding RNA in brain function and disease. Mol. Psychiatr. 19, 410–416.

Bertram, J., Fulton, B., Tourigny, J.P., Pena-Garcia, Y., Moyle, L.C., Hahn, M.W., 2023. CAGEE: computational analysis of gene expression evolution. Mol. Biol. Evol. 40.

Bi, X., Zhou, L., Zhang, J.J., Feng, S., Hu, M., Cooper, D.N., Lin, J., Li, J., Wu, D.D., Zhang, G., 2023. Lineage-specific accelerated sequences underlying primate evolution. Sci. Adv. 9, eadc9507.

Bryleva, E.Y., Rogers, M.A., Chang, C.C., Buen, F., Harris, B.T., Rousselet, E., Seidah, N.G., Oddo, S., LaFerla, F.M., Spencer, T.A., et al., 2010. ACAT1 gene ablation increases 24(S)-hydroxycholesterol content in the brain and ameliorates amyloid pathology in mice with AD. Proc. Natl. Acad. Sci. U. S. A. 107, 3081–3086.

Callaway, E.M., Dong, H.-W., Ecker, J.R., Hawrylycz, M.J., Huang, Z.J., Lein, E.S., Ngai, J., Osten, P., Ren, B., Tolias, A.S., et al., 2021. A multimodal cell census and atlas of the mammalian primary motor cortex. Nature 598, 86–102.

Cardenas-Navia, L.I., Cruz, P., Lin, J.C., Program, N.C.S., Rosenberg, S.A., Samuels, Y., 2010. Novel somatic mutations in heterotrimeric G proteins in melanoma. Cancer Biol. Ther. 10, 33–37.

Carroll, S.B., 2008. Evo-devo and an expanding evolutionary synthesis: a genetic theory of morphological evolution. Cell 134, 25–36.

Cohen, J.S., Srivastava, S., Farwell, K.D., Lu, H.M., Zeng, W., Lu, H., Chao, E.C., Fatemi, A., 2015. *ELP2* is a novel gene implicated in neurodevelopmental disabilities. Am. J. Med. Genet. 167, 1391–1395.

Daneshmandpour, Y., Darvish, H., Emamalizadeh, B., 2018. *RIT2*: responsible and susceptible gene for neurological and psychiatric disorders. Mol. Genet. Genom. 293, 785–792.

Du, J., Zhu, Z., Xu, L., Chen, X., Li, X., Lan, T., Li, W., Yuan, K., Zeng, Y., 2020. ARHGEF11 promotes proliferation and epithelial-mesenchymal transition of hepatocellular carcinoma through activation of β-catenin pathway. Aging (Albany NY) 12, 20235–20253.

Einarsdottir, E., Svensson, I., Darki, F., Peyrard-Janvid, M., Lindvall, J.M., Ameur, A., Jacobsson, C., Klingberg, T., Kere, J., Matsson, H., 2015. Mutation in *CEP63* cosegregating with developmental dyslexia in a Swedish family. Hum. Genet. 134, 1239–1248.

Elmentaite, R., Dominguez Conde, C., Yang, L., Teichmann, S.A., 2022. Single-cell atlases: shared and tissue-specific cell types across human organs. Nat. Rev. Genet. 23, 395–410.

Fay, J.C., Wittkopp, P.J., 2008. Evaluating the role of natural selection in the evolution of gene regulation. Heredity 100, 191–199.

Fraser, H.B., 2011. Genome-wide approaches to the study of adaptive gene expression evolution: systematic studies of evolutionary adaptations involving gene expression will allow many fundamental questions in evolutionary biology to be addressed. Bioessays 33, 469–477.

Gao, X., Wang, S., Wang, Y.F., Li, S., Wu, S.X., Yan, R.G., Zhang, Y.W., Wan, R.D., He, Z., Song, R.D., et al., 2022. Long read genome assemblies complemented by single cell RNA-sequencing reveal genetic and cellular mechanisms underlying the adaptive evolution of yak. Nat. Commun. 13, 4887.

Geirsdottir, L., David, E., Keren-Shaul, H., Weiner, A., Bohlen, S.C., Neuber, J., Balic, A., Giladi, A., Sheban, F., Dutertre, C.A., et al., 2019. Cross-species single-cell analysis reveals divergence of the primate microglia program. Cell 179, 1609–1622.

Gilad, Y., Oshlack, A., Rifkin, S.A., 2006a. Natural selection on gene expression. Trends Genet. 22, 456–461.

Gilad, Y., Oshlack, A., Smyth, G.K., Speed, T.P., White, K.P., 2006b. Expression profiling in primates reveals a rapid evolution of human transcription factors. Nature 440, 242–245.

Gilbert, N.M., O'Brien, V.P., Waller, C., Batourina, E., Mendelsohn, C.L., Lewis, A.L., 2022. *Gardnerella* exposures alter bladder gene expression and augment uropathogenic *Escherichia coli* urinary tract infection in mice. Front. Cell. Infect. Microbiol. 12, 909799.

Guo, J., Higginbotham, H., Li, J., Nichols, J., Hirt, J., Ghukasyan, V., Anton, E.S., 2015. Developmental disruptions underlying brain abnormalities in ciliopathies. Nat. Commun. 6, 7857.

Hao, Y., Hao, S., Andersen-Nissen, E., Mauck, W.M., Zheng, S., Butler, A., Lee, M.J., Wilk, A.J., Darby, C., Zager, M., et al., 2021. Integrated analysis of multimodal single-cell data. Cell 184, 3573–3587.

He, M., Pei, Z., Mohsen, A.W., Watkins, P., Murdoch, G., Van Veldhoven, P.P., Ensenauer, R., Vockley, J., 2011. Identification and characterization of new long chain acyl-CoA dehydrogenases. Mol. Genet. Metabol. 102, 418–429.

Heimer, G., Gregory, A., Hogarth, P., Hayflick, S., Ben Zeev, B., 1993. *MECR*-related neurologic disorder. In: Adam, M.P., Feldman, J., Mirzaa, G.M., Pagon, R.A., Wallace, S.E., Amemiya, A. (Eds.), Genereviews®. Seattle (WA).

Hilton, H.G., Rubinstein, N.D., Janki, P., Ireland, A.T., Bernstein, N., Fong, N.L., Wright, K.M., Smith, M., Finkle, D., Martin-McNulty, B., et al., 2019. Single-cell transcriptomics of the naked mole-rat reveals unexpected features of mammalian immunity. PLoS Biol. 17, e3000528.

Ho, W.C., Ohya, Y., Zhang, J., 2017. Testing the neutral hypothesis of phenotypic evolution. Proc. Natl. Acad. Sci. U. S. A. 114, 12219–12224.

Hodge, R.D., Bakken, T.E., Miller, J.A., Smith, K.A., Barkan, E.R., Graybuck, L.T., Close, J.L., Long, B., Johansen, N., Penn, O., et al., 2019. Conserved cell types with divergent features in human versus mouse cortex. Nature 573, 61–68.

Hodgins-Davis, A., Rice, D.P., Townsend, J.P., 2015. Gene expression evolves under a house-of-cards model of stabilizing selection. Mol. Biol. Evol. 32, 2130–2140.

Hu, J., Liao, J., Sathanoori, M., Kochmar, S., Sebastian, J., Yatsenko, S.A., Surti, U., 2015. *CNTN6* copy number variations in 14 patients: a possible candidate gene for neurodevelopmental and neuropsychiatric disorders. J. Neurodev. Disord. 7, 26.

Hudson, R.R., Kreitman, M., Aguade, M., 1987. A test of neutral molecular evolution based on nucleotide data. Genetics 116, 153–159.
Jorstad, N.L., Song, J.H.T., Exposito-Alonso, D., Suresh, H., Castro-Pacheco, N., Krienen, F.M., Yanny, A.M., Close, J., Gelfand, E., Long, B., et al., 2023. Comparative transcriptomics reveals human-specific cortical features. Science 382, eade9516.
Katzman, A., Alberini, C.M., 2018. NLGN1 and NLGN2 in the prefrontal cortex: their role in memory consolidation and strengthening. Curr. Opin. Neurobiol. 48, 122–130.
Keough, K.C., Whalen, S., Inoue, F., Przytycki, P.F., Fair, T., Deng, C., Steyert, M., Ryu, H., Lindblad-Toh, K., Karlsson, E., et al., 2023. Three-dimensional genome rewiring in loci with human accelerated regions. Science 380, eabm1696.
Khaitovich, P., Hellmann, I., Enard, W., Nowick, K., Leinweber, M., Franz, H., Weiss, G., Lachmann, M., Paabo, S., 2005. Parallel patterns of evolution in the genomes and transcriptomes of humans and chimpanzees. Science 309, 1850–1854.
King, M.C., Wilson, A.C., 1975. Evolution at two levels in humans and chimpanzees. Science 188, 107–116.
Kojic, M., Gawda, T., Gaik, M., Begg, A., Salerno-Kochan, A., Kurniawan, N.D., Jones, A., Drozdzyk, K., Koscielniak, A., Chramiec-Glabik, A., et al., 2021. *Elp2* mutations perturb the epitranscriptome and lead to a complex neurodevelopmental phenotype. Nat. Commun. 12, 2678.
La Manno, G., Gyllborg, D., Codeluppi, S., Nishimura, K., Salto, C., Zeisel, A., Borm, L.E., Stott, S.R.W., Toledo, E.M., Villaescusa, J.C., et al., 2016. Molecular diversity of midbrain development in mouse, human, and stem cells. Cell 167, 566–580.
Lee, D., Shahandeh, M.P., Abuin, L., Benton, R., 2025. Comparative single-cell transcriptomic atlases of drosophilid brains suggest glial evolution during. ecological adaptation. PLoS Biol. 23, e3003120.
Lehner, B., 2008. Selection to minimise noise in living systems and its implications for the evolution of gene expression. Mol. Syst. Biol. 4, 170.
Liao, B.Y., Zhang, J., 2006. Low rates of expression profile divergence in highly expressed genes and tissue-specific genes during mammalian evolution. Mol. Biol. Evol. 23, 1119–1128.
Lin, T.D., Rubinstein, N.D., Fong, N.L., Smith, M., Craft, W., Martin-McNulty, B., Perry, R., Delaney, M.A., Roy, M.A., Buffenstein, R., 2024. Evolution of T cells in the cancer-resistant naked mole-rat. Nat. Commun. 15, 3145.
Lu, F., Shen, S.H., Wu, S., Zheng, P., Lin, K., Liao, J., Jiang, X., Zeng, G., Wei, D., 2022. Hypomethylation-induced prognostic marker zinc finger DHHC-type palmitoyltransferase 12 contributes to glioblastoma progression. Ann. Transl. Med. 10, 334.
Luo, R., Fan, Y., Yang, J., Ye, M., Zhang, D.F., Guo, K., Li, X., Bi, R., Xu, M., Yang, L.X., et al., 2021. A novel missense variant in ACAA1 contributes to early-onset Alzheimer's disease, impairs lysosomal function, and facilitates amyloid-β pathology and cognitive decline. Signal Transduct. Targeted Ther. 6, 325.
Ma, S., Skarica, M., Li, Q., Xu, C., Risgaard, R.D., Tebbenkamp, A.T.N., Mato-Blanco, X., Kovner, R., Krsnik, Ž., de Martin, X., et al., 2022. Molecular and cellular evolution of the primate dorsolateral prefrontal cortex. Science 377, eabo7257.
Manceau, M., Domingues, V.S., Mallarino, R., Hoekstra, H.E., 2011. The developmental role of Agouti in color pattern evolution. Science 331, 1062–1065.
Mascheretti, S., Riva, V., Giorda, R., Beri, S., Lanzoni, L.F., Cellino, M.R., Marino, C., 2014. *KIAA0319* and *ROBO1*: evidence on association with reading and pleiotropic effects on language and mathematics abilities in developmental dyslexia. J. Hum. Genet. 59, 189–197.
Metzger, B.P., Yuan, D.C., Gruber, J.D., Duveau, F., Wittkopp, P.J., 2015. Selection on noise constrains variation in a eukaryotic promoter. Nature 521, 344–347.
Mizuno, Y., Ninomiya, Y., Nakachi, Y., Iseki, M., Iwasa, H., Akita, M., Tsukui, T., Shimozawa, N., Ito, C., Toshimori, K., et al., 2013. Tysnd1 deficiency in mice interferes with the peroxisomal localization of PTS2 enzymes, causing lipid metabolic abnormalities and male infertility. PLoS Genet. 9, e1003286.
Murat, F., Mbengue, N., Winge, S.B., Trefzer, T., Leushkin, E., Sepp, M., Cardoso-Moreira, M., Schmidt, J., Schneider, C., Mossinger, K., et al., 2023. The molecular evolution of spermatogenesis across mammals. Nature 613, 308–316.
Necsulea, A., Kaessmann, H., 2014. Evolutionary dynamics of coding and non-coding transcriptomes. Nat. Rev. Genet. 15, 734–748.
Niepoth, N., Merritt, J.R., Uminski, M., Lei, E., Esquibies, V.S., Bando, I.B., Hernandez, K., Gebhardt, C., Wacker, S.A., Lutzu, S., et al., 2024. Evolution of a novel adrenal cell type that promotes parental care. Nature 629, 1082–1090.
Oegema, R., Baillat, D., Schot, R., van Unen, L.M., Brooks, A., Kia, S.K., Hoogeboom, A.J.M., Xia, Z., Li, W., Cesaroni, M., et al., 2017. Human mutations in integrator complex subunits link transcriptome integrity to brain development. PLoS Genet. 13, e1006809.
Pan, X., Zhao, J., Zhou, Z., Chen, J., Yang, Z., Wu, Y., Bai, M., Jiao, Y., Yang, Y., Hu, X., et al., 2021. 5'-UTR SNP of *FGF13* causes translational defect and intellectual disability. Elife 10, e63021.
Paradis, E., Schliep, K., 2019. Ape 5.0: an environment for modern phylogenetics and evolutionary analyses in R. Bioinformatics 35, 526–528.
Plass, M., Solana, J., Wolf, F.A., Ayoub, S., Misios, A., Glazar, P., Obermayer, B., Theis, F.J., Kocks, C., Rajewsky, N., 2018. Cell type atlas and lineage tree of a whole complex animal by single-cell transcriptomics. Science 360, eaaq1723.
Price, P.D., Palmer Droguett, D.H., Taylor, J.A., Kim, D.W., Place, E.S., Rogers, T.F., Mank, J.E., Cooney, C.R., Wright, A.E., 2022. Detecting signatures of selection on gene expression. Nat. Ecol. Evol. 6, 1035–1045.
Quinlan, A.R., Hall, I.M., 2010. BEDTools: a flexible suite of utilities for comparing genomic features. Bioinformatics 26, 841–842.
Qureshi, I.A., Mehler, M.F., 2011. Non-coding RNA networks underlying cognitive disorders across the lifespan. Trends Mol. Med. 17, 337–346.
Raj, A., Rifkin, S.A., Andersen, E., van Oudenaarden, A., 2010. Variability in gene expression underlies incomplete penetrance. Nature 463, 913–918.
Regev, A., Teichmann, S.A., Lander, E.S., Amit, I., Benoist, C., Birney, E., Bodenmiller, B., Campbell, P., Carninci, P., Clatworthy, M., et al., 2017. The human cell atlas. Elife 6, e27041.
Ren, Y., Qian, Y., Ai, L., Xie, Y., Gao, Y., Zhuang, Z., Chen, J., Chen, Y.X., Fang, J.Y., 2021. TRAPPC 4 regulates the intracellular trafficking of PD-L1 and antitumor immunity. Nat. Commun. 12, 5405.
Rifkin, S.A., Kim, J., White, K.P., 2003. Evolution of gene expression in the *Drosophila melanogaster* subgroup. Nat. Genet. 33, 138–144.
Rohlfs, R.V., Nielsen, R., 2015. Phylogenetic ANOVA: the expression variance and evolution model for quantitative trait evolution. Syst. Biol. 64, 695–708.
Rohlfs, R.V., Harrigan, P., Nielsen, R., 2014. Modeling gene expression evolution with an extended Ornstein-Uhlenbeck process accounting for within-species variation. Mol. Biol. Evol. 31, 201–211.
Ross-Gillespie, A., O'Riain, M.J., Keller, L.F., 2007. Viral epizootic reveals inbreeding depression in a habitually inbreeding mammal. Evolution 61, 2268–2273.
Sackton, T.B., Grayson, P., Cloutier, A., Hu, Z., Liu, J.S., Wheeler, N.E., Gardner, P.P., Clarke, J.A., Baker, A.J., Clamp, M., et al., 2019. Convergent regulatory evolution and loss of flight in paleognathous birds. Science 364, 74–78.
Salta, E., De Strooper, B., 2017. Noncoding RNAs in neurodegeneration. Nat. Rev. Neurosci. 18, 627–640.
Shafer, M.E.R., Sawh, A.N., Schier, A.F., 2022. Gene family evolution underlies cell-type diversification in the hypothalamus of teleosts. Nat. Ecol. Evol. 6, 63–76.
Shao, Y., Zhou, L., Li, F., Zhao, L., Zhang, B.-L., Shao, F., Chen, J.-W., Chen, C.-Y., Bi, X., Zhuang, X.-L., et al., 2023. Phylogenomic analyses provide insights into primate evolution. Science 380, 913–924.
Signor, S.A., Nuzhdin, S.V., 2018. The evolution of gene expression in *cis* and *trans*. Trends Genet. 34, 532–544.
St Pourcain, B., Cents, R.A., Whitehouse, A.J., Haworth, C.M., Davis, O.S., O'Reilly, P.F., Roulstone, S., Wren, Y., Ang, Q.W., Velders, F.P., et al., 2014. Common variation near *ROBO2* is associated with expressive vocabulary in infancy. Nat. Commun. 5, 4831.
Sun, M., Zhang, J., 2020. Allele-specific single-cell RNA sequencing reveals different architectures of intrinsic and extrinsic gene expression noises. Nucleic Acids Res. 48, 533–547.
Suresh, H., Crow, M., Jorstad, N., Hodge, R., Lein, E., Dobin, A., Bakken, T., Gillis, J., 2023. Comparative single-cell transcriptomic analysis of primate brains highlights human-specific regulatory evolution. Nat. Ecol. Evol. 7, 1930–1943.
The Tabula Muris Consortium, 2018. Single-cell transcriptomics of 20 mouse organs creates a *Tabula Muris*. Nature 562, 367–372.
Tosches, M.A., Yamawaki, T.M., Naumann, R.K., Jacobi, A.A., Tushev, G., Laurent, G., 2018. Evolution of pallium, hippocampus, and cortical cell types revealed by single-cell transcriptomics in reptiles. Science 360, 881–888.
Wang, J., Sun, H., Jiang, M., Li, J., Zhang, P., Chen, H., Mei, Y., Fei, L., Lai, S., Han, X., et al., 2021. Tracing cell-type evolution by cross-species comparison of cell atlases. Cell Rep. 34, 108803.
Waskom, M.L., 2021. Seaborn: statistical data visualization. J. Open Source Softw. 6, 3021.
Whitehead, A., Crawford, D.L., 2006. Variation within and among species in gene expression: raw material for evolution. Mol. Ecol. 15, 1197–1211.
Wu, X., Jiang, L., Qi, H., Hu, C., Jia, X., Lin, H., Wang, S., Lin, L., Zhang, Y., Zheng, R., et al., 2024. Brain tissue- and cell type-specific eQTL Mendelian randomization reveals efficacy of *FADS1* and *FADS2* on cognitive function. Transl. Psychiatry 14, 77.
Xie, X., Shi, Q., Wu, P., Zhang, X., Kambara, H., Su, J., Yu, H., Park, S.Y., Guo, R., Ren, Q., et al., 2020. Single-cell transcriptome profiling reveals neutrophil heterogeneity in homeostasis and infection. Nat. Immunol. 21, 1119–1133.
Ximerakis, M., Lipnick, S.L., Innes, B.T., Simmons, S.K., Adiconis, X., Dionne, D., Mayweather, B.A., Nguyen, L., Niziolek, Z., Ozek, C., et al., 2019. Single-cell transcriptomic profiling of the aging mouse brain. Nat. Neurosci. 22, 1696–1708.
Yang, J., Ruan, H., Xu, W., Gu, X., 2019. TreeExp2: an integrated framework for phylogenetic transcriptome analysis. Genome Biol. Evol. 11, 3276–3282.
Yeh, M.L., Gonda, Y., Mommersteeg, M.T., Barber, M., Ypsilanti, A.R., Hanashima, C., Parnavelas, J.G., Andrews, W.D., 2014. Robo1 modulates proliferation and neurogenesis in the developing neocortex. J. Neurosci. 34, 5717–5731.
Youn, Y.H., Han, Y.G., 2018. Primary cilia in brain development and diseases. Am. J. Pathol. 188, 11–22.
Yu, G., Wang, L.G., Han, Y., He, Q.Y., 2012. clusterProfiler: an R package for comparing biological themes among gene clusters. OMICS 16, 284–287.
Zhang, J., Yang, J.R., 2015. Determinants of the rate of protein sequence evolution. Nat. Rev. Genet. 16, 409–420.
Zhang, Y., Koe, C.T., Tan, Y.S., Ho, J., Tan, P., Yu, F., Sung, W.K., Wang, H., 2019. The integrator complex prevents dedifferentiation of intermediate neural progenitors back into neural stem cells. Cell Rep. 27, 987–996.
Zhang, Y., Hill, C.M., Leach, K.A., Grillini, L., Deliard, S., Offley, S.R., Gatto, M., Picone, F., Zucco, A., Gardini, A., 2025. The enhancer module of integrator controls cell identity and early neural fate commitment. Nat. Cell Biol. 27, 103–117.
Zhuang, X.L., Zhang, J.J., Shao, Y., Ye, Y., Chen, C.Y., Zhou, L., Wang, Z.B., Luo, X., Su, B., Yao, Y.G., et al., 2023. Integrative omics reveals rapidly evolving regulatory sequences driving primate brain evolution. Mol. Biol. Evol. 40, msad173.